The Atlantic Ocean's Decadal Variability in mid-Holocene Simulations using Shannon's Entropy

Iuri Gorenstein[1], Ilana Wainer[1], Francesco S. R. Pausata[2], Luciana F. Prado[3], Pedro L. Silva Dias[4], Allegra N. LeGrande[5], Clay R. Tabor[6], and William R. Peltier[7]

[1]Departamento de Oceanografia Física, São Paulo, SP, Brazil
[2]Centre ESCER (Etude et la Simulation du Climat à l'Echelle Regionale) and GEOTOP (Research Center on the Dynamics of the Earth System), Department of Earth and Atmospheric Sciences, University of Quebec, Montreal, Montreal, QC, Canada
[3]Faculdade de Oceanografia, Universidade do Estado do Rio de Janeiro, Rio de Janeiro, Brazil
[4]Instituto de Astronomia, Geofísica e Ciências Atmosféricas, Universidade de São Paulo, Departamento de Ciências Atmosféricas, São Paulo, Brazil
[5]NASA Goddard Institute for Space Studies, and Center for Climate Systems Research, Columbia University, New York, USA
[6]Department of Geosciences, University of Connecticut, USA
[7]Department of Physics, University of Toronto, Canada

Correspondence: Iuri Gorenstein (iuri.gorenstein@usp.br)

Abstract. ~~Accurate simulation of mean climate and variability is crucial for numerical climate models. Traditional methods assess variability using two-dimensional standard deviation fields, like sea surface temperature (SST) and precipitation, to identify key regions. However, this approach can overlook large-scale patterns, such as ocean modes of variability, used in traditional climatology and oceanography to define climate variability.~~ Quantifying climate variability in a way that is comparable across models, experiments, and observations remains challenging, particularly at decadal time scales where nonlinear dynamics dominate. Traditional variance-based metrics are sensitive to anomaly amplitude, mean-state biases, and units of measurement, limiting their robustness for inter-model analyses. Here, we introduce an information-theoretic framework that characterizes climate variability as trajectories in a discrete phase space and quantifies system organization using Shannon's entropy. ~~We propose a method incorporating large-scale climate patterns to evaluate and compare decadal variability in~~ Using four coupled models (EC-Earth, GISS, iCESM, and CCSM-Toronto)~~. Shannon's Entropy compares the models' sensitivity to different scenarios: pre-industrial period, mid-Holocene with default vegetation, ~~, we apply our methodology to compare the models' tropical and South Atlantic decadal variability, analyzing their sea surface temperature (SST) and precipitation under Pre-Industrial and mid-Holocene ~~with prescribed Green Sahara conditions. Results show contrasting model responses, with little consensus on the effects of Green Sahara vegetation and orbital forcing. Three models (EC-Earth, iCESM, and CCSM-Toronto) show reduced precipitation variability under Green Sahara conditions, but with differing SST responses. The GISS model shows minimal effects on variability. Additionally, reducing dust in the Green Sahara scenario significantly impacted ~~boundary conditions, including Green Sahara experiments, and compare the results with observational datasets. Mid-Holocene forcings lead to model-dependent entropy changes, indicating a reorganization of Atlantic decadal variability rather than a uniform response across models. Green Sahara boundary conditions reduced SST entropy in EC-Earth ~~'s model, increasing precipitation while decreasing SST variability~~and GISS models, implying a more organized Atlantic system, while

precipitation responses are more heterogeneous. Entropy values derived from principal-component-based phase spaces have shown a more consistent framework to compare numerical models varaibility with observational estimates than using the traditional regional SST boxes index-based phase space. These findings highlight the diverse representations of climate variability across models~~and offer a new methodology for comprehensive model analysis.~~ . As such, this framework enables robust comparisons of low-frequency climate variability across models, paleoclimate simulations, and observations, complementing traditional variance-based diagnostics.

1 Introduction

A system's variability can be perceived as the absence of uniformity across multi-scales (Sang, 2013). Earth's climate can be interpreted as a ~~high dimensional~~ high-dimensional chaotic system (highly ~~dependant~~ dependent on initial conditions), ~~with many feedbacks and interactions among an extensive set of particles and radiation (Ghil and Lucarini, 2020; Kwiecien et al., 2022) . Since this system is in constant motion, climate internal variability denotes how we perceive the climate system driven by its intrinsic dynamics, regardless of any transient external forcings (Flato et al., 2014). Numerical climate models are used to extrapolate our limited observational data set and study not only the climate's internal variability, but its changes, and debate past and future scenarios of Earth's climate .~~ and understanding the structure and drivers of climate variability remains a central challenge in climate science, particularly at decadal time scales where internal dynamics and external forcings interact in nonlinear ways. (Ghil and Lucarini, 2020; Kwiecien et al., 2022). Traditional approaches to characterizing variability often rely on variance-based metrics or spectral analyses, which are sensitive to amplitude, mean-state biases, and the choice of variables or units (Ghil et al., 2002; Froyland et al., 2021). While these methods have been important in identifying dominant modes of variability, they provide limited insight into how climate systems explore their range of possible states, how persistent those states are, and how transitions between them evolve under different climate forcings Sane et al. (2024).

~~The study of interannual precipitation patterns in the~~ The tropical and South Atlantic ~~regions~~ Ocean (15N - 30S, 60W-20E, region defined in the maps ~~from Figs. 3, 4~~ 'a' ~~), as well as the adjacent continents, provides critical insight into the dynamics~~ and 'b' from Figs. 1) play a fundamental role in regulating global climate through their influence on the interhemispheric energy balance, the position of the Intertropical Convergence Zone, ~~one of the most distinctive characteristics of Earth's climate variability. This major zone of convection and surface wind convergence is significantly influenced by variations in wind, sea level pressure, and~~ and the coupling between sea surface temperature (SST) ~~gradients, which can displace the zone both within and across hemispheres~~ and precipitation.(Dhrubajyoti et al., 2019; Hounsou-Gbo et al., 2019; Atwood et al., 2020). ~~Such variations are key not only on an annual scale but also have important implications for decadal precipitation changes, further modulated by the ocean's modes of variability , such as the Atlantic Equatorial Mode (AEM), Atlantic Meridional Mode (AMM) and South Atlantic Subtropical Dipole (Gorenstein et al., 2023). Oscillating at lower frequencies, these modes play an essential role in the displacement of convergence zones (Deser et al., 2010). The interaction between oceanand atmospheric dynamics, rooted in non-linear processes within large-scale climate phenomena, establishes a robust coupling between precipitation and SST on a decadal scale. This complex relationship underscores~~ Decadal variability in

this region is associated with large-scale Atlantic modes that modulate rainfall over South America and Africa and interact with both extratropical and tropical circulation patterns (Gorenstein et al., 2023). Because these modes arise from coupled ocean–atmosphere processes, changes in their organization or persistence can have far-reaching climatic impacts (Deser et al., 2010), while underscoring the difficulty in predicting ~~precipitation and SST anomalies~~ their evolution due to their reliance on a wide range of interacting climate variables (Deser et al., 2012).

~~Studying past climates is a practical way to apply numerical climate models to study diverse equilibrium states of Earth's climate. In the~~ The mid-Holocene (MH) period, approximately 5000-7000 years Before Present, ~~we observe a climate characterized by differential summer insolation across hemispheres, leading to the "Holocene Thermal Maximum" (Berger, 1988; Liu et al., 2002; Bova e . Despite its potential as an analog for future climate scenarios (Burkea et al., 2018; Kaufman et al., 2020), the warming~~ provides a natural framework to investigate how external forcings reshape climate variability. Orbital changes during this period ~~was neither uniform across the globe nor consistent throughout the year, exhibiting notable disparities across hemispheres and seasons (Berger, 1978; Zhao and Harrison, 2012; Huo et al., 2021). This period saw an intensification of monsoon systems in the Northern Hemisphere, while precipitation in the Southern Hemisphere was reduced compared to the present day (Liu et al., 2004; Wanner et al., 2008; Smith and Mayle, 2017). Furthermore, other climate forcings and feedbacks played an important role during the MH, such as~~ altered the seasonal and latitudinal distribution of insolation, leading to profound hydroclimatic changes (Berger, 1988; Liu et al., 2002; Bova et al., 2021), most notably the African Humid Period and the expansion of vegetation ~~in areas that are currently deserted in northern Africa (the Green Sahara - GS) and Asia. Such changes had a remarkable impact on global temperature and precipitation patterns and contributed to an intensification of the Atlantic Meridional Overturning Circulation, impacting vegetation in regions dependent on the South American summer monsoon, such as the southwest Amazon and parts of Brazil (Smith and Mayle, 2017; Gorenstein et al., 2022a)~~over the Sahara (Demenocal et al., 2000). Proxy studies and climate model simulations suggest that these boundary-condition changes affected not only mean climate states but also the dynamics of tropical and Atlantic variability through land–atmosphere–ocean feedbacks (Pausata et al., 2016; Smith and Mayle, 2017; Gorenstein et al., 2022a). Rather than simply amplifying or damping anomalies, quantifying how such forcings reorganize decadal variability remains an open problem, particularly when comparing across models with differing physics and parameterizations.

The geophysical mechanisms behind the Atlantic Ocean modes coupling with pressure and wind driving decadal precipitation anomalies were unraveled using observational data in Gorenstein et al. ~~, 2023~~(2023). When examining ~~this region's dynamics~~ the dynamics of this region in climate simulations, a more fundamental question arose regarding how to assess its decadal variability. Since numerical models present biased climate representations compared to observational data and among themselves (Dhrubajyoti et al., 2019), their climate variability is not ~~usually measured concerning large climate patterns~~typically measured in relation to large-scale climate patterns, such as ocean modes~~, instead, it is measured using point-wise standard deviation and frequency spectra (Olonscheck and Notz, 2017; Pendergrass et al., 2017)~~. This motivated us to create a new method using ocean modes and their precipitation counterparts to quantify decadal variability in numerical climate models.

In this study, we ~~define climate variability with concepts from statistical mechanics, oceanography, and climatology. Applying Shannon'~~adopt an alternative perspective grounded in information theory to characterize climate variability as the evolution of

a system through a discrete phase space. By representing SST and precipitation anomalies as trajectories in low-dimensional spaces and applying Shannon's entropy to measure the organization of the Atlantic Ocean modes and their precipitation counterparts~~, we compare climate variability among different numerical models and scenarios. Simulations from four different Earth System Models (EC-Earth, iCESM, CCSM-Toronto, and GISS) are analyzed to study pre-industrial (PI) climate~~. This framework allows us to compare Pre-Industrial and mid-Holocene ~~(MH) experiments. The MH experiments include conditions with (MH_{GS}) and without (MH_{PMIP}) vegetation changes in northern Africa~~climate simulations across multiple models, as well as ~~experiments incorporating parametrized changes in dust reduction, lake extensions, and soil moisture levels (see Methods)~~observational datasets, within a unified and scale-invariant metric. By doing so, we aim to assess how mid-Holocene forcings reshape the persistence and transitions of dominant Atlantic climate states, offering a complementary and physically interpretable measure of climate variability beyond traditional variance-based approaches.

2 Material and Methods

Simulations from four numerical climate models (EC-Earth, iCESM, CCSM-Toronto, and GISS) are used to study decadal climate variability of the tropical and South Atlantic (25°N-45°S,60°W-20°E) Sea Surface Temperature (SST) and precipitation, ~~and its sensibility~~ as well as their sensitivity to prescribed parametrizations~~in~~. The simulations are separated into pre-industrial ~~(PI)and~~ boundary conditions (PI), simulations using mid-Holocene ~~(MH)simulations~~insolation boundary conditions (MH_{PMIP}), and simulations using mid-Holocene insolation and different vegetation inputs (MH_{GS}). Details defining each numerical simulation are described below.

2.1 Data

EC-Earth

The European Consortium Earth System Model Version-3 (EC-Earth) scenarios analyzed in this study were: ~~PI~~ PI (100 years run B405 and 200 years run B400), MH_{PMIP} (100 years run Z6KA and 200 years run B6KA), MH_{GS} (100 years run G105 and 50 years run G100, simulations with prescribed vegetation in the Sahara region) and MH_{GSdr} ~~with dust reduction~~ (100-year run G506, and 200-year run G501,simulations with prescribed vegetation in the Sahara region and dust reduction).

EC-Earth standard configuration consists of the atmosphere model IFS, including the land surface module HTESSEL and the ocean model NEMO3.6 with the sea ice module LIM3. Coupling variables are communicated between the different component models via the OASIS3-MCT coupler (Döscher et al., 2021). The EC-Earth model is used to contribute to CMIP6 in several configurations, for example, the EC-Earth3-Veg configuration, which couples the LPJ-Guess dynamic vegetation model (Smith et al., 2014) to the atmosphere and ocean model~~; however~~. However, the performance of EC-Earth3 and EC-Earth3-Veg is very similar (Wyser et al., 2020).

CESM models

The Community Earth System Model (CESM) outputs from different scenarios used were from CCSM-Toronto: ~~PI, MH, GS, and GS with~~ PI, MH_{PMIP}, MH_{GS}, and MH_{GSsl} (with prescribed soil and lake ~~input (~~inputs), 100 years run each~~)~~; and iCESM: ~~PI~~PI, MH_{PMIP}, MH_{GS} (100 years run each).

The CESM models used here are from the ~~Cmip6~~ CMIP6 multi-model ensemble. The CCSM-Toronto simulations are a PMIP experiment for the mid-Holocene with Green Sahara and mid-Holocene with soil and lake inputs made by the University of Toronto (UofT), Canada. The model configuration was made by UofT-CCSM4 (2014), atmosphere from CAM4 (finite-volume dynamical core; 288 x 192 longitude/latitude; 26 levels; top level 2 hPa) (Peltier and Vettoretti, 2014); ocean: POP2; sea ice: CICE4; land: CLM4. The iCESM simulations used in this study were first presented in Tabor et al. (2020). iCESM is configured with CAM5, POP2, CLM4, CICE4, and RTM (Brady et al., 2019; Hurrell et al., 2013). The atmosphere and land have a 1.9 × 2.5° horizontal resolution, and the ocean and sea ice have a nominal 1° horizontal resolution. Model configurations include a preindustrial simulation (1850 CE), a mid-Holocene simulation with a 6-ka orbit and greenhouse gases and preindustrial vegetation, and a mid-Holocene Green Sahara simulation with a 6-ka orbit and greenhouse gases and a vegetated Sahara. Dust emissions from the Sahara are reduced in the mid-Holocene Green Sahara simulation. For additional model configuration details, see Tabor et al. (2020).

GISS

The scenarios from the Goddard Institute for Space Studies Model E2 coupled with the Russel ocean model (GISS-E2-R) were: ~~PI, H_{PMIP}, and MH_{GS}~~ PI, MH_{PMIP}, and MH_{GSNA} with North African vegetation only, MH_{GSEX} with Extra-Tropical vegetation only, and two runs of MH_{GSALL} with Full vegetation (100 years run each).

All runs—except for GS Full Vegetation Run 1—use updated aerosol and ozone inputs for non-anthropogenic simulations and apply the Green Sahara vegetation based on Nancy Kiang's regression on leaf area index (Kiang, 2002). In contrast, GS Full Vegetation Run 1 employs a regression script based on the Köppen–Geiger classification to prescribe the leaf area index (Sohoulande, 2023). Several experiments have been set up for the last millennium with GISS due to uncertainties in past forcings and their effects, with different combinations of solar, volcanic, and land use/vegetation (Colose et al., 2016; LeGrande et al., 2015; Bühler et al., 2022).

~~Low frequency filters~~GPCP

~~To study the decadal variability of the Atlantic Ocean, decadal filters were applied to all data sets. These filters are calculated with the simple decadal mean from the original monthly time series~~ The Global Precipitation Climatology Project (GPCP) is a precipitation dataset based on the sequential combination of microwave, infrared, and gauge data. From 1979 to 2020, and offers globally complete satellite-only precipitation estimates (Sun et al., 2017). To examine the precipitation over the Atlantic in the satellite era and compare its Shannon Entropy values to the ones calculated using model simulations, we utilized

the GPCP Version 2.3 Combined Precipitation dataset (Adler et al., 2003). This dataset provides both continental and ocean precipitation data in a monthly, 2,5°x2,5° grid, during the 1979-2015 period.

HADISST

The observational sea surface data comes used is from Met Office Hadley Centre's sea ice and sea surface temperature dataset (HadISST1), a monthly 1°x1° dataset (Rayner et al., 2003a), which is a Reanalysis dataset that uses observational data from ship expeditions and platforms interpolated by a numerical model to recreate the Global SST. The sea surface temperature anomaly was calculated with respect to the 1979-2015 period. To separate the Atlantic SST anomaly pattern of variability from any global warming signal, the mean global temperature anomaly was also calculated and subtracted from the SST anomaly time series (Zhang et al., 1997; Mantua et al., 1997; Bonfils and Santer, 2011).

In this study, the HadISST1 dataset has been used to measure the values of Entropy from the observational data using the phase space retrieved from the merged simulations dataset. While historical climate model simulations are best suited for comparisons with observational data, this study focuses on pre-industrial and mid-Holocene scenarios. Nevertheless, we applied our methodology to satellite data to quantify Shannon's Entropy for the observational period.

Table 1: Data used in this study

Model/Dataset	Experiments/Period	Reference
EC-Earth	PI,MH,MH_{GS},MH_{GSdr} (dust reduction)	Döscher et al. (2021)
iCESM	PI,MH,MH_{GS}	Tabor et al. (2020)
CCSM-Toronto	PI,MH,MH_{GS},MH_{GSsl} (soil and lake)	Peltier and Vettoretti (2014)
GISS	PI,MH,MH_{GS},MH_{GSna} (North Africa vegetation) MS_{GSex}, MH_{GSall} (Extra-tropical and Full vegetation)	Schmidt et al. (2014)
HadISST1	$1979-2015$	Rayner et al. (2003b)
GPCP	$1979-2015$	Adler et al. (2003)

2.2 Methods

~~**Principal Component Analysis and the phase space**~~

Climate systems are inherently high-dimensional, making their direct analysis challenging. To address this, we apply dimensionality reduction, a standard procedure that projects the system into a lower-dimensional space (a.k.a phase space) while retaining its essential dynamics. In this reduced representation, the climate system evolves along a trajectory. By constructing such trajectories for different climate systems within the same reduced space, we obtain a common framework for comparison. These trajectories encapsulate key aspects of climate variability and dynamical periodicity, which can then be systematically analyzed across systems. In this section, we will present a simplified 2-dimensional solution for the tropical and South Atlantic SST system, enabling us to apply our method more comprehensively.

2.2.1 Dimensionality Reduction - Defining the Phase Space

Principal Component Analysis

~~The~~ Principal Component (PC) analysis (also known as Empirical Orthogonal Functions - EOF) is a technique used to reduce data dimensionality. When studying a ~~high-dimension stochastic~~ high-dimensional dynamical system, such as numerical climate model simulations, finding relevant statistical information ~~emerging from the physics of the system~~that emerges from the system's dynamics can be inefficient and overwhelming (Haykin, 2009). The PC analysis derives a new set of orthogonal coordinates from your data, ~~maximizing the variance from each component~~ ordering the EOF patterns that maximize the data's variance in a decreasing fashion, enabling a drastic ~~dimensionality reduction of your data set while preserving~~ reduction in dimensionality of your dataset while preserving most of its variation (Jolliffe, 2002). The PC time series is the projection of our data in the corresponding EOF pattern.

~~There are three main ocean~~ In this approach, we extracted two distinct phase spaces (one for SST and another for precipitation) composed of EOFs derived from the combined simulations of all models and scenarios. This process yields a unified phase space with a shared spatial structure for the entire ensemble, providing a consistent framework for analyzing and comparing variability across different simulations (Chandler et al., 2024). This procedure is discussed and applied by Chandler et al. (2024), who construct a merged dataset across models and extract dominant modes of variability ~~controlling the decadal climate~~ using principal component analysis. Their approach implicitly defines a shared low-dimensional representation for inter-model comparison, which is conceptually related to our phase-space construction.

Low frequency filters

To investigate decadal variability in the ~~tropical and South Atlantic region~~ Atlantic Ocean, decadal filters were applied across all datasets, calculated as simple decadal means from the original monthly time series. These filters serve two primary purposes: first, to examine the decadal coupling between precipitation and SST variables; and second, to extract consistent multi-model patterns that serve as the foundation for a shared phase space. Decadal filtering is applied to the precipitation and SST datasets before pattern extraction to effectively smooth out fine-scale structures and disparities arising from different

model architectures. Since we define a single phase space to encompass the merged dataset, this filtering process is essential to ensure that the leading climatic patterns capture substantial variance across the integrated multi-model ensemble.

Atlantic Ocean Modes SST Indices

A more classical approach to reducing the dimensionality of Atlantic Ocean SST and identifying its modes of variability is through the use of SST indices from regional boxes (Deser et al., 2010). Together with pressure gradients and wind anomalies, ~~they~~ the ocean modes arising from these SST anomalies induce precipitation in the ocean and adjacent continents (Gorenstein et al., 2023). ~~We represent the data using the three leading principal components of sea surface temperature and precipitation in the~~ These indices are constructed from pre-defined spatial boxes and provide a reduced representation of the system by capturing key patterns of tropical and South Atlantic ~~. Together, these components explain about~~ SST decadal variability. In particular, the Atlantic Meridional Mode (AMM: the difference between 15°–5°N, 50~~% of the total variance across all simulations (21% from the first PC, 17% from the second, and 12% from the third). While PC patterns can vary between model simulations and may not exactly match observations, we limit our analysis to three components based on their established physical relevance as drivers of observed decadal variability in the region. This also avoids the complexity of working in higher-dimensional phase space and ensures our analysisremains grounded in physically meaningful modes.~~

~~In this approach, we extracted two distinct PC phase spaces from the dataset: one for SST and another for precipitation. Each PC phase space consists of the three principal components derived from the combined simulations, encompassing all models and scenarios. This process results in a unified 3-dimensional phase space for each variable, providing a consistent framework to analyze and compare the variability across different simulations~~°–20°W and 15°–5°S, 20°W–10°E regional boxes), the Atlantic Equatorial Mode (AEM: 3°N-3°S, 20°-0°W regional box), and the South Atlantic Subtropical Dipole (SASD: the difference between 30°–40°S, 10°–30°W and 15°–25°S, 0°–20°W regional boxes) can be used to define a phase space analogous to that obtained via PC analysis. However, unlike the PC analysis, these indices can be highly correlated, and they have no reciprocal precipitation modes. In our study, this framework is used to compare the system's decadal SST variability using different techniques to define the phase-space.

~~**The trajectories in phase space**~~

2.2.2 The trajectories in phase space

Projecting a simulation series onto the 'n' ~~principal components of the set of simulations~~ dimensions of our phase space generates a trajectory in ~~an n-dimensional phase space(not shown). This trajectory is determined by the continuous PC indices (~~that phase space. To elaborate more, we present a simplified 2-dimensional phase space for the SST decadal anomalies of the EC-Earth - PI experiment, using the two leading EOFs from the merged dataset. First, we apply the dimensionality reduction using the PC analysis to find the merged dataset two leading EOFs (Figure 1 'a' ~~in Figs. 3 and 4).~~ and 'b'). Then, we project the EOFs into the simulation's Atlantic Ocean time series, generating its PCs (Figure 1 'c' and 'd'). The trajectory of our system in the 2-D continuous phase space is shown in Figure 1 'f'. Defining negative, neutral, and positive phases for each ~~index using~~

index, using a threshold linked to Shannon's Entropy (as described in Section 2.3)~~., we discretize~~ , we coarse-grain this space into n^3 states ~~.~~

~~Since we choose to represent the tropical and South Atlantic system with its 3 main components, our discrete phase space is a set of 27 possible states for SST and 27~~ (9 possible states for ~~precipitation (Figure S1 from Supplementary Material). The trajectories of each simulation run in~~ this 2-D problem). The discrete state evolution of our system (Figure 1 'e') is defined by quadrants in the 2-D map (States from Figure 1 'f'). Finally, the trajectory can also be seen as a discrete system evolving in time, from one possible state to the next, as depicted in Figure 1 'g'.

Since the continuous trajectory in a high-dimensional phase space can be challenging to plot, the trajectories of a system in a higher-dimensional phase space can be depicted with directed graphs (~~'b' in Figs.~~ Figure 2; 'h' in Figures 3 and 4~~).~~ ; and Figures 5-8). These graphs can hold different information regarding the system's trajectory in phase space. Each node in these graphs represents a state of the system at a particular time step, with the node's size indicating the number of months the system remained in that state. Nodes that appear darker have a higher degree, meaning they are connected to more transitions to and from other states. This indicates that the system frequently returns to the same state, which results in a darker color for that node. The distance between nodes is irrelevant~~,~~ ; it was adjusted ~~accordingly to depict~~ for the graph. The information in a directed graph can be overwhelming to analyze for every simulation run~~,~~ ; therefore, we ~~use~~ utilize its information to calculate a macro-property ~~reflecting their~~ that reflects its variability in phase space.

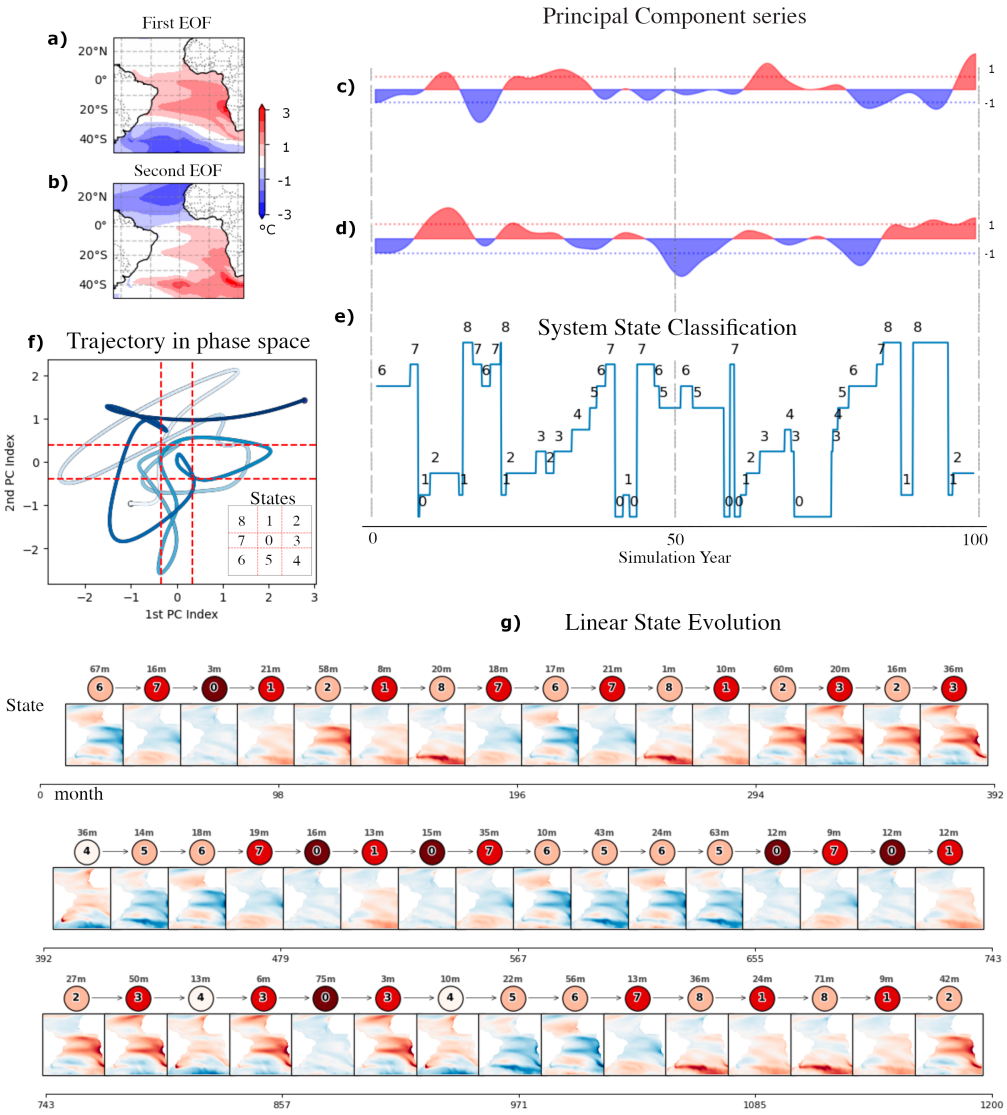

Figure 1. EC-Earth SST system state identification and evolution during the PI experiment. a) ~~the three principal components~~ The first EOF; b) The second EOF; (~~PCs~~c) ~~indexes~~ and (d): their respective PC series, blue for negative and red for positive, dashed lines indicating the 1 standard deviation value. ~~From top to bottom~~(e) The cluster identification of the discrete system state, given by the ~~AEM~~ two PC indices above. (~~first component~~f) The system's trajectory in the continuous PC phase space. The line's color represents the time evolution, ~~AMM~~ white for the start (~~second Component~~month 0) ~~,~~ and ~~SASD~~ dark blue for its end (~~third component~~month 1200). ~~b~~(g) ~~To the right,~~ The diagram illustrates the ~~cluster identification~~ state-by-state evolution of the system ~~state given~~ over time. Each node represents a specific SST pattern, identified by its cluster number (referenced in panels (e) and (f)) and its spatial pattern displayed below the ~~three above PC indexes~~node. ~~To~~ The numeral positioned above each node indicates the ~~left~~duration, ~~the cluster identification of~~ in months, that the system remained in that state ~~is represented by a directed graph~~before transitioning. ~~Each~~ Darker shading on a node signifies a higher frequency of transitions into that specific ~~state, as depicted in Figure S1 from Supplementary Material~~cluster throughout the entire time series.

~~EC-Earth precipitation system state identification and evolution during the PI experiment. a) the three principal components (PCs) indexes~~

~~Entropy as an analogue for climate variability~~

2.2.3 Entropy as an analogue for climate variability

Shannon's Entropy (equation 1) is used ~~in this study to measure the variability from each simulation in~~ as a measure of variability in unfied the phase space~~by attributing its trajectory with an entropy value~~.

$$H = -\sum_{k=1}^{k=0} {}^{N} P(x_k) ln(P(x_k)) \quad (1)$$

The entropy of a dynamic system is a measure of ~~organization~~its organization in a coarse-grained space. For example, the systems from Fig. 2 'a' and 'b' have the same initial and final states (0 and 4, respectively)~~,~~; however, system 'a' evolves directly from the initial to the final state, while system 'b' varies across different states until arriving at the final state. This means that system 'a' is less chaotic, its trajectory is more organized, and hence its entropy is smaller.

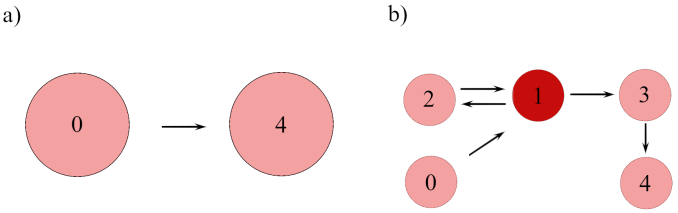

Figure 2. Two abstract directed graphs representing dynamic systems of the same time series length: a) A system evolves from its initial state (0) to its final state (4) — a low-entropy system. b) A system evolves from its initial state (0) to state 1, then to state 2, back to state 1, to state 3, and finally to its final state (4) — a high-entropy system.

Looking at equation 1, the probability ($P(x_k)$) of our system x (the simulated Atlantic Ocean SST and precipitation) being found in each possible state (k) can be calculated empirically from the simulation time series. For example, if a specific simulation has been in only one state during its whole time series, that state (x_k) has a probability equal to one to be found in that specific state and zero ~~on~~ in the others. Considering that $\sum_{k=1}^{N} P(x_k) = 1$, the entropy from that time series is the lowest possible, zero. ~~Using the~~ In our study, defining a 3-dimensional phase space and discretizing each dimension in 3 possible phases (positive, negative, or neutral) creates 27 ~~states from the discrete PC phase space as the~~ possible states of our system~~, the~~. The entropy from each time series will reflect its variability in that discrete phase space. Since we are using the same space for all the models and scenarios, we can compare their variability.

From a broader perspective, the probability distribution from the Atlantic SST or precipitation patterns (micro-states) in a simulation (trajectory) is used to determine the ~~systems'~~system's decadal variability (macro-properties) ~~.~~

2.3 ~~Proposed approach for measuring uncertainty~~

There are a few sources of uncertainty when calculating entropy from numerical climate model outputs. Numerical models inherently involve: (i) internal variability - the general climate variability at pre-industrial or other standard scenarios -; (ii) differences in numerical discretization - which shape how physical processes are represented -; and (iii) scenario-based uncertainty (Lehner et al., 2020). Our analysis focuses on variability emerging from the discrete PC phase space representation. Since we use a in our unified phase space for all models and scenarios, our calculated entropy reflects differences in how each simulation explores this unified space. The uncertainty in entropy is derived empirically, based on how entropy depends on the PC space and the threshold values used. While (the 3 leading EOFs from our merged dataset).

2.3 Phase-Space Discretization Based on Maximum Entropy

The results presented in this study are based on a multi-model analysis using single realizations from each experiment. Because we do not explicitly separate internal variability, discretization, and scenario uncertainty, our approach indirectly captures elements of all three. However, since we are not using a large ensemble, our conclusions are limited to the specific simulations analyzed.

In this study, we did not compare observational data to the model output patterns, but, in theory, we could. In this scope, the observational data variability and the different model scenarios variability could be compared using the same methodology. Furthermore, the observation and model representations need to be balanced when defining a common PC phase space . This space creates the base where the system will be projected, and later, the trajectories and entropy will be calculated. If biased systems are compared, it is best to balance the data set used to derive the PCs, otherwise, instead of a trajectory's organization, a low entropy may reflect the absence of analyze large ensembles of simulations, the conclusions drawn here are strictly conditional on the specific models and experiments considered. Within this context, the uncertainty associated with the entropy estimates arises primarily from the discretization of the principal-component phase space and the representation of its variation in the PC phase space27 possible states.

The Possible States of the Tropical and South Atlantic system

The choice of representing our system with the 3-dimensional PC space was based on previous literature about how the modes of variability work at decadal time scales. The decadal SST patterns known as modes of variability are correlated to the ocean and continental precipitation such that these patterns' feedback and interaction with each other are the main drivers of the Tropical and South Atlantic decadal variability (Gorenstein et al., 2023). By using this PC space we are discussing numerical model variability at different experiments with the same metrics used to discuss observational data variability.

Entropy's Maximum and its Uncertainty

Entropy is an emergent property of the 3-dimensional PC phase space . A common way The value of Shannon's entropy depends critically on how the phase space is discretized. Small changes in the thresholds used to define the positive, negative, and neutral phases of each PC index is to apply a fixed threshold, such as half a standard deviation. However, small changes

~~in this threshold can significantly alter the~~ can substantially alter a simulation's trajectory through phase space and~~thus affect~~ , consequently, its entropy (see Figures S2 and S3 ~~from~~ in the Supplementary Material). ~~Instead of using a fixed rule, we identify, for each simulation, the threshold that yields the maximum entropy—i.e.~~ A common approach in the literature is to normalize each principal component by its standard deviation and apply a fixed threshold to define these phases (typically ranging between 0.5 and 1.5). However, climate models differ markedly in their representation of variability due to internal climate fluctuations, differences in numerical formulation and parameterizations, and uncertainties associated with imposed boundary conditions and forcings (Lehner et al., 2020). Applying a single fixed threshold across all models, therefore, risks producing entropy values that reflect differences in simulated amplitudes rather than differences in the temporal organization of variability.

To address this limitation, we adopt an entropy-centered discretization strategy in which the threshold is determined by the requirement of maximizing entropy, rather than prescribing entropy as a consequence of an arbitrary threshold choice. In this formulation, the threshold ~~that results in the greatest diversity of system states during the simulation. This "maximum entropy" reflects the most representative variabilityfor that simulation. Because this ideal threshold varies between simulations , we use each simulation~~is allowed to vary between simulations, ensuring that each model's ~~maximum entropy as a consistent basis for comparing variability. We estimate the uncertainty of this value~~ s variability is characterized using the discretization that best represents its exploration of the phase space.

All simulations are projected onto a unified phase space, such that differences in entropy arise solely from how each simulation occupies and transitions between the same set of possible system states. Although we do not explicitly disentangle the relative contributions of internal variability, model structure, and scenario forcing, these effects are implicitly encoded and absorved by this mobile threshold and in the resulting state trajectories. Given the limited number of simulations analyzed, the results should be interpreted as conditional on the specific models and experiments considered, rather than as a comprehensive sampling of model uncertainty.

The maximum entropy of a trajectory is an emergent property of the three-dimensional phase space and corresponds to the threshold that yields the greatest diversity of occupied system states during a simulation. The uncertainty associated with this estimate is quantified using a bootstrap approach.

~~In~~ For each simulation, entropy is evaluated over an interval of ~~ideal thresholds was applied~~ candidate thresholds used to define the 27 possible ~~states according to the intensity of the three PCs~~system states associated with the three principal components. The maximum entropy ~~value was attributed to~~ is identified for each time series, and ~~a bootstrap technique was used to define its 95% confidence interval (the percentile bootstrap interval) (Hinkley, 1988; Diciccio and Romano, 1988; Gorenstein et al., 2022 . To calculate this confidence interval, we augmented our data using only our pre-existing dataset for~~ its uncertainty is estimated using a percentile bootstrap method (Hinkley, 1988; Diciccio and Romano, 1988; Gorenstein et al., 2022b). Specifically, 1000 surrogate realizations of each phase space index are generated by resampling from the original dataset of each experiment, and ~~, with this augmented data set, 1000 PC indexes were generated, from which we calculated their maximum entropy and their~~ the maximum entropy is recalculated for each realization. The resulting 95% confidence interval ~~. This confidence interval was~~

is taken as the uncertainty ~~from each trajectory's entropy and used to discuss the climate variability of each simulation run~~of the entropy estimate and is used to assess differences in climate variability between simulations.

In climatology, variability encompasses the temporal amplitude fluctuations of a given variable. In contrast, Shannon Entropy, as calculated here, accounts for these variations with an amplitude filter. When we define a phase space using the leading PCs, we select a domain characterized by the patterns representing the system's greatest variance. By normalizing the indices and determining the threshold that maximizes Shannon Entropy, we effectively isolate temporal dynamics from the influence of amplitude variations. Our approach establishes a leveled ground for analyzing the temporal evolution of the system's state across its defining patterns, ensuring that the results remain independent of the specific amplitude differences simulated by various numerical models. In other words, although two models may reproduce the 1st PC with different amplitudes, they are both considered representations of the same climatic pattern. Consequently, Shannon's Entropy evaluates the system's persistence and transitions between states independently of these amplitude variations.

3 Results

We test our methodology in three steps. First, we analyze the outputs of four different numerical climate models in PI and various MH climate scenarios (see Methods). We extract the tropical and South Atlantic SST and precipitation three leading Principal Components (PCs), calculate their trajectory in this 3-dimensional phase space, and compute their respective Shannon Entropy. In the second, we explore the classical Oceanography SST-based indexes to create the Tropical and South Atlantic Ocean's SST phase space (see Methods), calculate its trajectory and Shannon Entropy once again. The third step is a comparison between the calculated entropy values from the model simulations and observational data from satellites using the previously discussed phase spaces.

3.1 The Green-Sahara Simulations in the Principal Component Phase Space

We define ~~our~~ the system as the ~~Tropical~~ coupled tropical and South Atlantic decadal ~~Sea Surface Temperature (SST)~~ variability of SST and precipitation. ~~We analyze monthly~~ Monthly outputs from 17 ~~simulation runs across different experiments, each spanning~~ simulations across multiple experiments are analyzed, each covering 1200 months on a one-degree resolution grid. ~~Therefore, each snapshot of the Tropical and South Atlantic has latitude and longitude dimensions of 80x89.~~ To ~~focus on the large climate patternsin our interest region and reduce the dimensionality in our data, we derive the three main Principal Components (PC) and use them to define two phase spaces, one for SST and another for precipitation. The PC analysis identifies the main patterns of our system's variability (Haykin, 2009). Furthermore, we project our system in these phase spaces, creating an index measuring the temporal evolution of each PC component during the simulation~~ (make sure we extract physically meaningful patterns, we create the merged data set's phase-space using the Tropical South Atlantic three leading EOFs (Figure 3, 'a' ~~from Figs. 3 and~~ a', 'b' and 'c') and project these spatial patterns in each simulations time series, creating their PCs (Figure 3, 'd', 'e' and 'f'), we repeat this procedure for precipitation (Figure 4). For SST, these components explain about 50% of the total variance across all simulations (21% from the first PC, 17% from the second, and 12% from the third). The three main components share the same spatial pattern as the detrended HadISST1 observation dataset (Rayner et al., 2003b), where they account for 80% of the total variance from 1979-2015 (42% from the first, 24% from the second, and 14% from the third - Figure S1).

~~When looking at the SST, the first three PCs are also known as the modes of variability of the Tropical and South Atlantic. The Atlantic Meridional Mode (AMM), the Atlantic Equatorial Mode (AEM), and the South Atlantic Subtropical Dipole (SASD). These modes' indexes represent our system in a low-dimensional phase space.~~ To transform this ~~space (the AMM, AEM, and SASD indexes)~~ continuous space into a discrete ~~representation~~space, we divide ~~the PC indexes~~ each PC index into three phases (positive, negative, and neutral), defining the 27 possible states in which our system's SST can be found (Figure ~~S1~~ S2 from Supplementary Material). ~~We expect precipitation and SST variabilities to be highly coupled at decadal time scale (Gorenstein et al., 2023). Therefore, analogous to the SST possible states, a construction is made using the first three PCs of precipitation. For SST and precipitation, the system state evolution throughout each simulation can be represented by a~~ , and constructing a discrete trajectory in phase space ~~.~~ ('g', 'h' and 'i' from Figure 3 and 4).

In Figs. 3 and 4, the EC-Earth PI experiment is used to illustrate how the PC ~~indexes~~ indices correlate with its trajectory. However, this choice is not particularly significant. All other graphs (Figs. 5, 6, 7, and 8) follow a similar construction and yield comparable results.

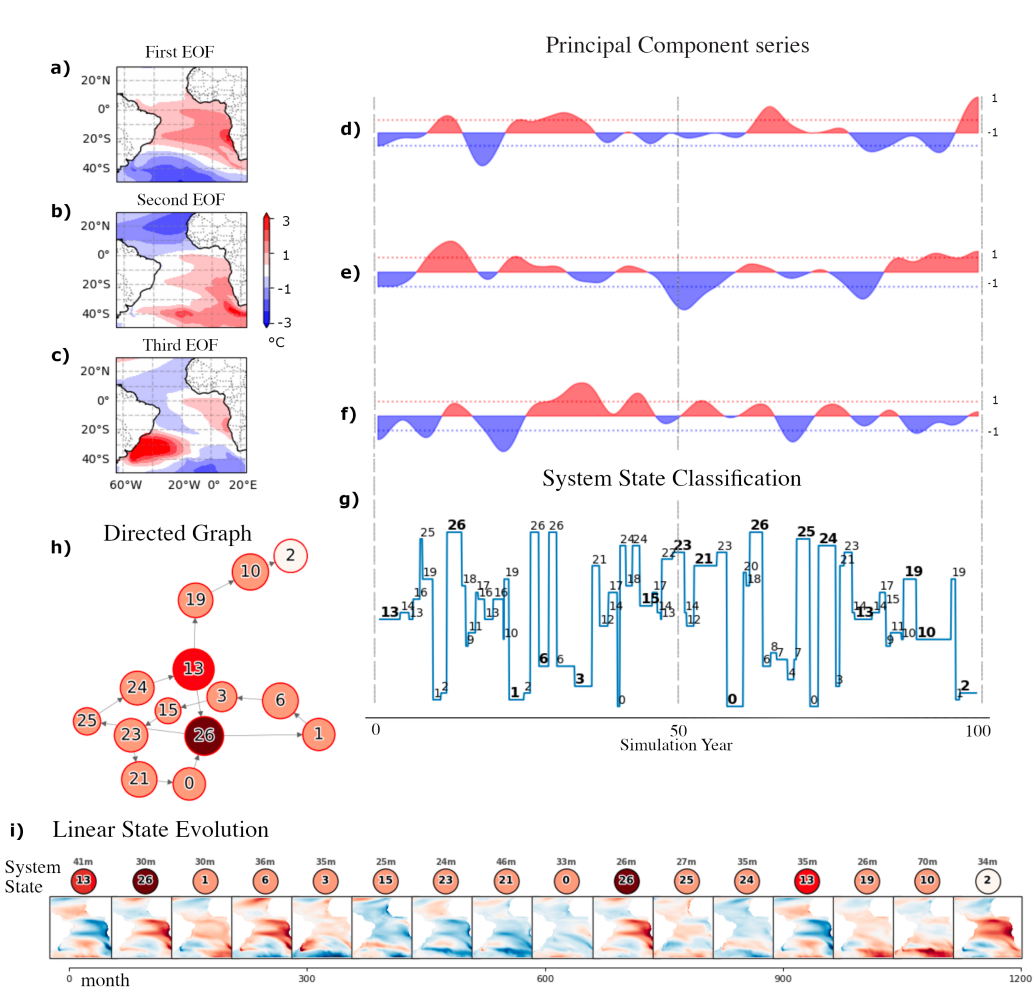

Figure 3. EC-Earth SST state identification and evolution during the PI experiment. Panels (a)–(c) show the merged ensemble's first three EOF patterns, with (d)–(f) displaying their corresponding PC series (red/blue indicating positive/negative phases; dashed lines showing 1 standard deviation). (g) identifies discrete system states based on these PC indices, bold font used in the most persistent states (lasting more than 24 months); (h) illustrates state evolution of the most persistent states. (i) tracks the state evolution in linear form. Each node displays its cluster number, spatial pattern, and duration in months before transitioning.

3.2 ~~Directed Graphs~~

~~As mentioned before, each~~

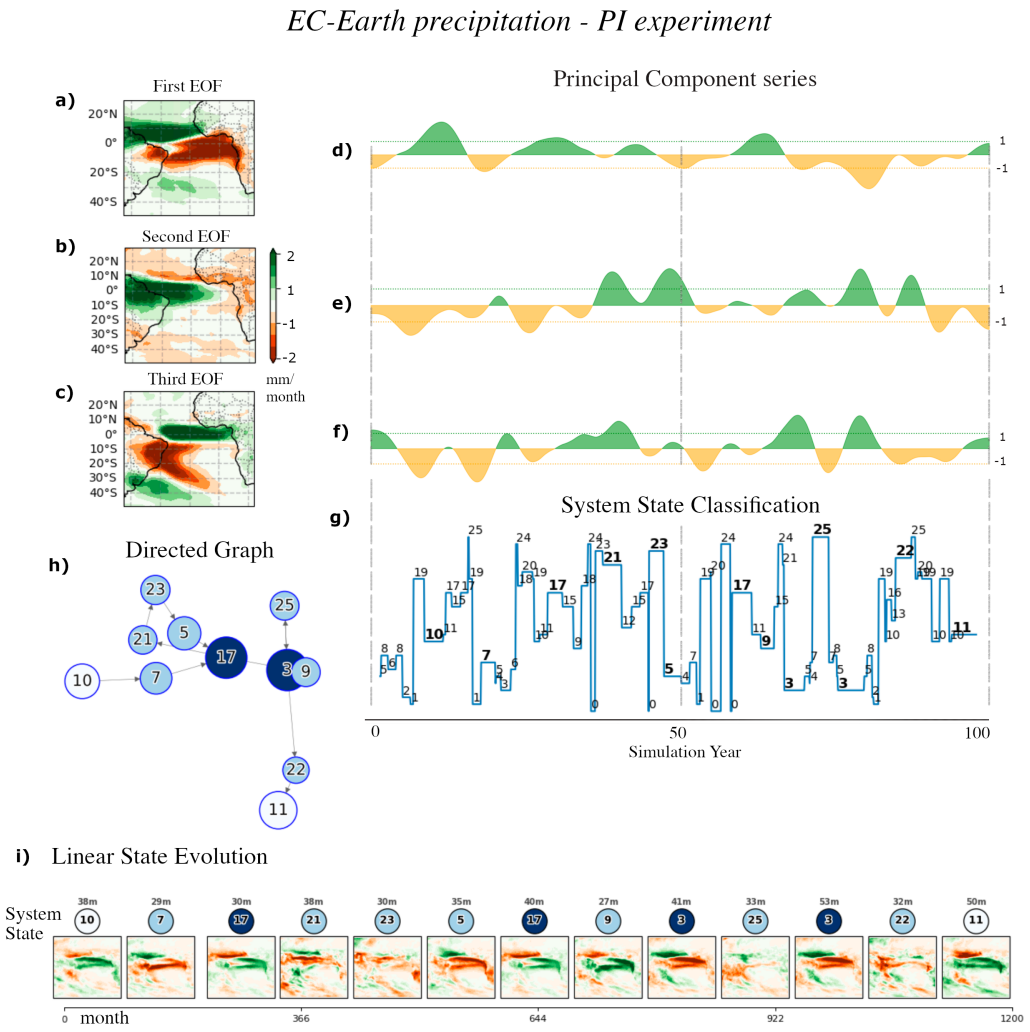

Figure 4. EC-Earth precipitation state identification and evolution during the PI experiment. Panels (a)–(c) show the merged ensemble's first three EOF patterns, with (d)–(f) displaying their corresponding PC series (green/orange indicating positive/negative phases; dashed lines showing 1 standard deviation). (g) identifies discrete system states based on these PC indices, bold font used in the most persistent states (lasting more than 24 months); (h) illustrates state evolution of the most persistent states. (i) tracks the state evolution in linear form. Each node displays its cluster number, spatial pattern, and duration in months before transitioning.

Directed Graphs

Each simulation run can be represented as two trajectories in the PC phase spaces, one for the SST and one for ~~the precipitation('b' from Figs.~~ precipitation. These trajectories of the Tropical and South Atlantic system (fully depicted for EC-Earth in the System State Classification 'g' from Figures 3 and 4) ~~. These trajectories of the Tropical and South Atlantic systems are represented as directed graphs in~~ are formed by all the states a system occupies during its time series. However, it can be challenging to present this information due to the high number of states and transistions. Even in a low 3-dimension phase space, it can be overwhelming to represent the full trajectory in a plain figure. Therefore, we chose to represent the most persistent states a system occupies (depicted in bold numbers in 'g' from Figures 3 and 4) in the directed graph form for each simulation experiment (Figs. 5 - 8). In Figures 3 and 4, the direct graph can be seen in its ciclycal and linear forms ('h' and 'i', respectively). These graphs qualitative ilustrate the ciclicity and organization of a simulation, furthermore, their construction uses quantitative measures of the system in the phase-space. Each node in these graphs represents a system state at a given time step, with its size ~~showing~~ indicating the duration spent in that state, and its color intensity reflecting the frequency of transitions to and from other states (higher degree). Darker nodes indicate states the system revisits more often.

~~The evolution in time of the EC-Earth PI in the SST and precipitation highlights the Atlantic Ocean decadal SST and precipitation cycles around a main pattern (cluster 0 - the PCs neutral pattern - Figure S1 from Supplementary Material).~~ The same properties used to design each graph ~~from Figs. 5 - 8~~ were employed to calculate macroproperties such as the entropy of the time series.

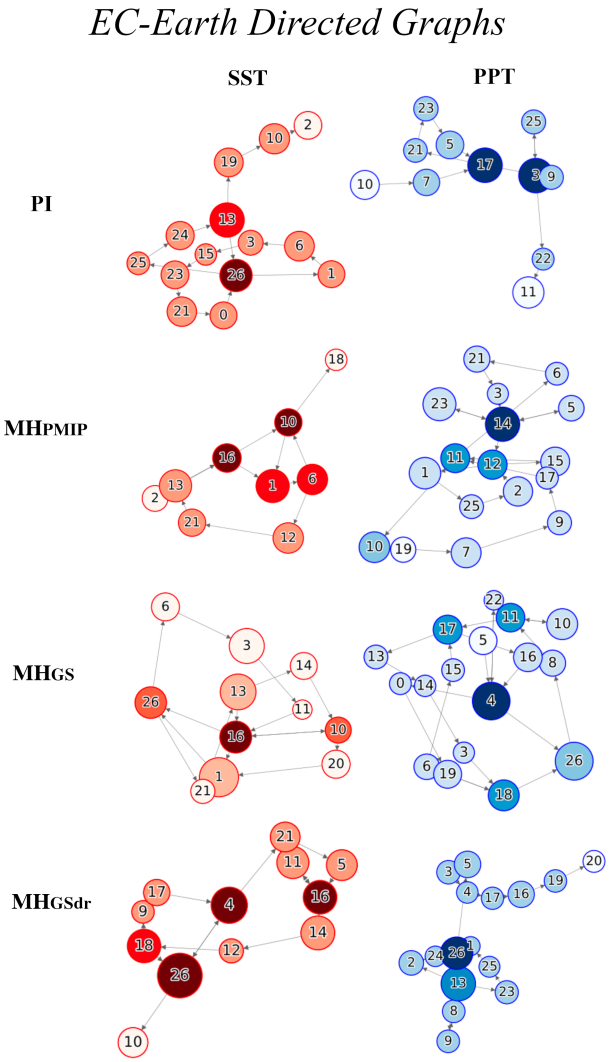

Figure 5. Directed graphs from EC-Earth - PI, MH_{PMIP}, MH_{GS}, and GS with dust reduction (MH_{GSdr}) simulations. The red graphs represent the SST system evolution, and the blue graphs represent the precipitation evolution. Each node signifies a specific state, as depicted in Figure ~~S1~~ S2 from the Supplementary Material.

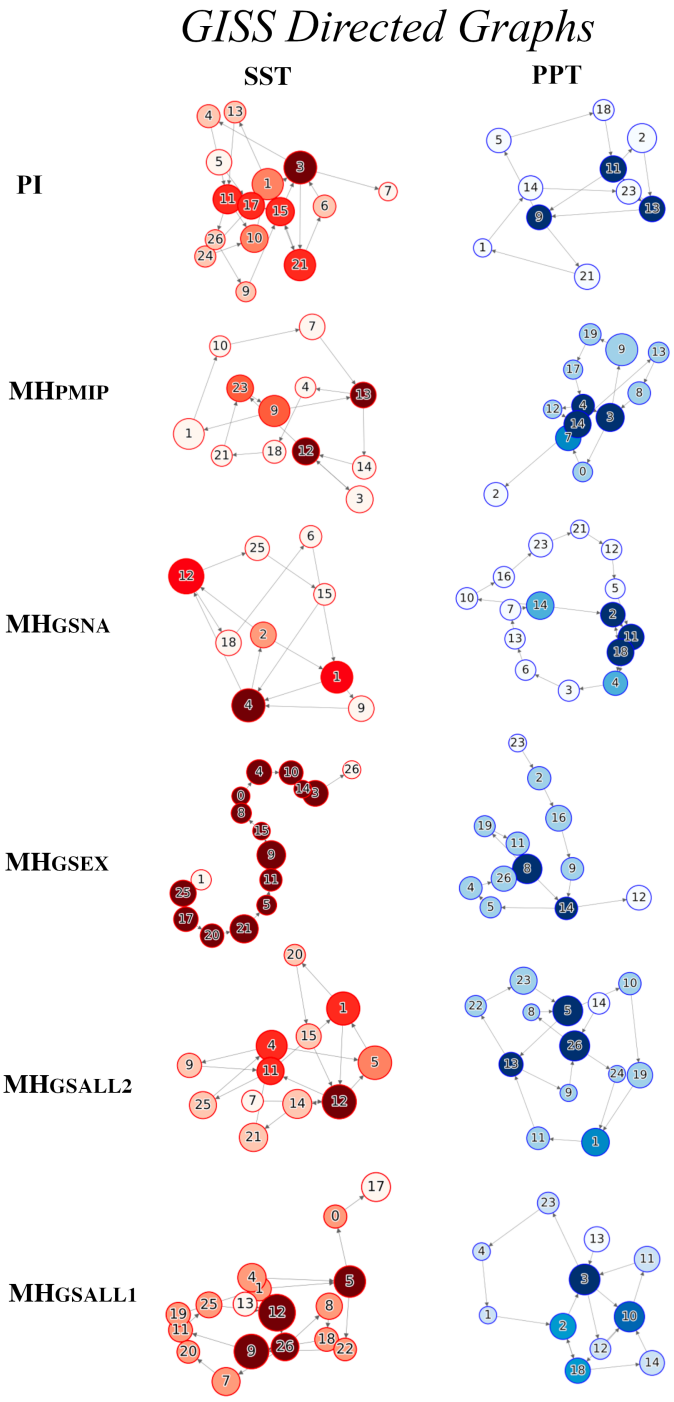

Figure 6. Directed graphs from GISS - PI, MH_{PMIP}, MH_{GS} with North Africa (MH_{GSNA}), Extra-Tropical (MH_{GSEX}), and full vegetation (MH_{GSALL1} and MH_{GSALL2}) runs. The red graphs represent the evolution of the SST system~~evolution~~, ~~and~~ while the blue graphs represent the ~~precipitation~~ evolution of precipitation. Each node signifies a specific state, as depicted in Figure ~~S1~~ S2 from the Supplementary Material.

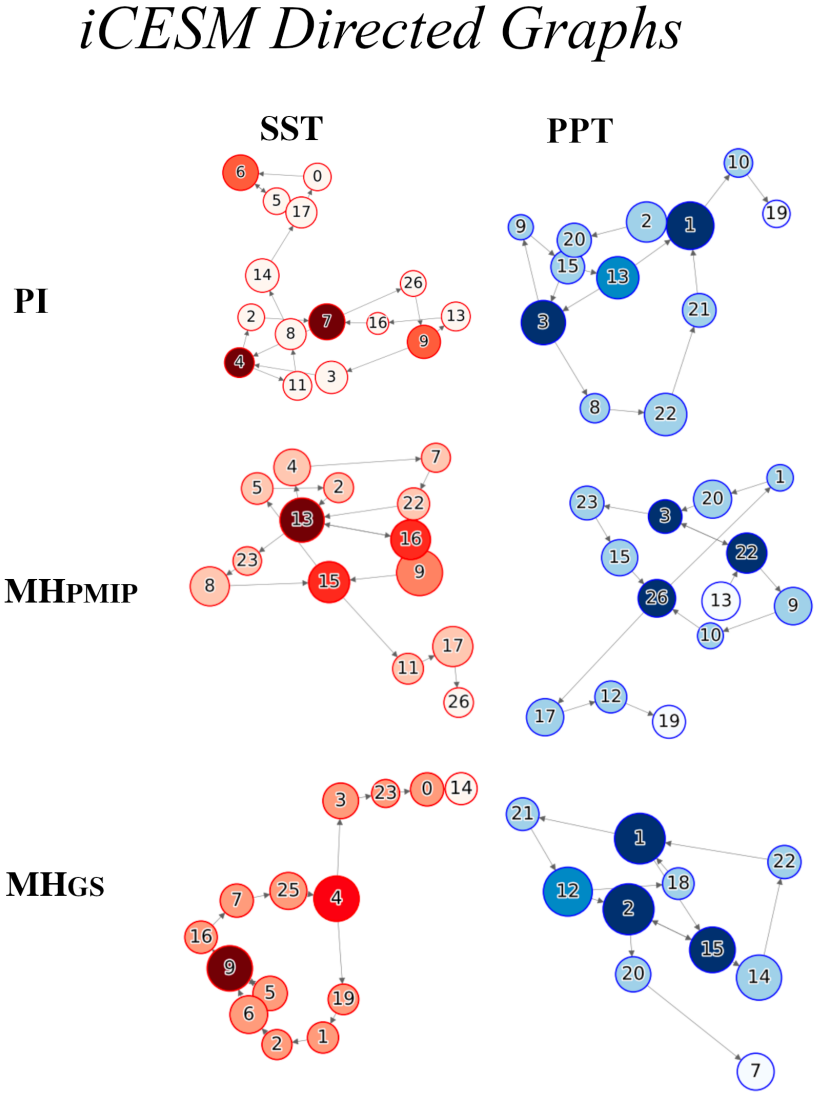

Figure 7. Directed graphs from iCESM - PI, MH_{PMIP}, and MH_{GS} runs. The red graphs represent the SST system evolution, and the blue graphs represent the precipitation evolution. Each node signifies a specific state, as depicted in Figure ~~S1~~ S2 from the Supplementary Material.

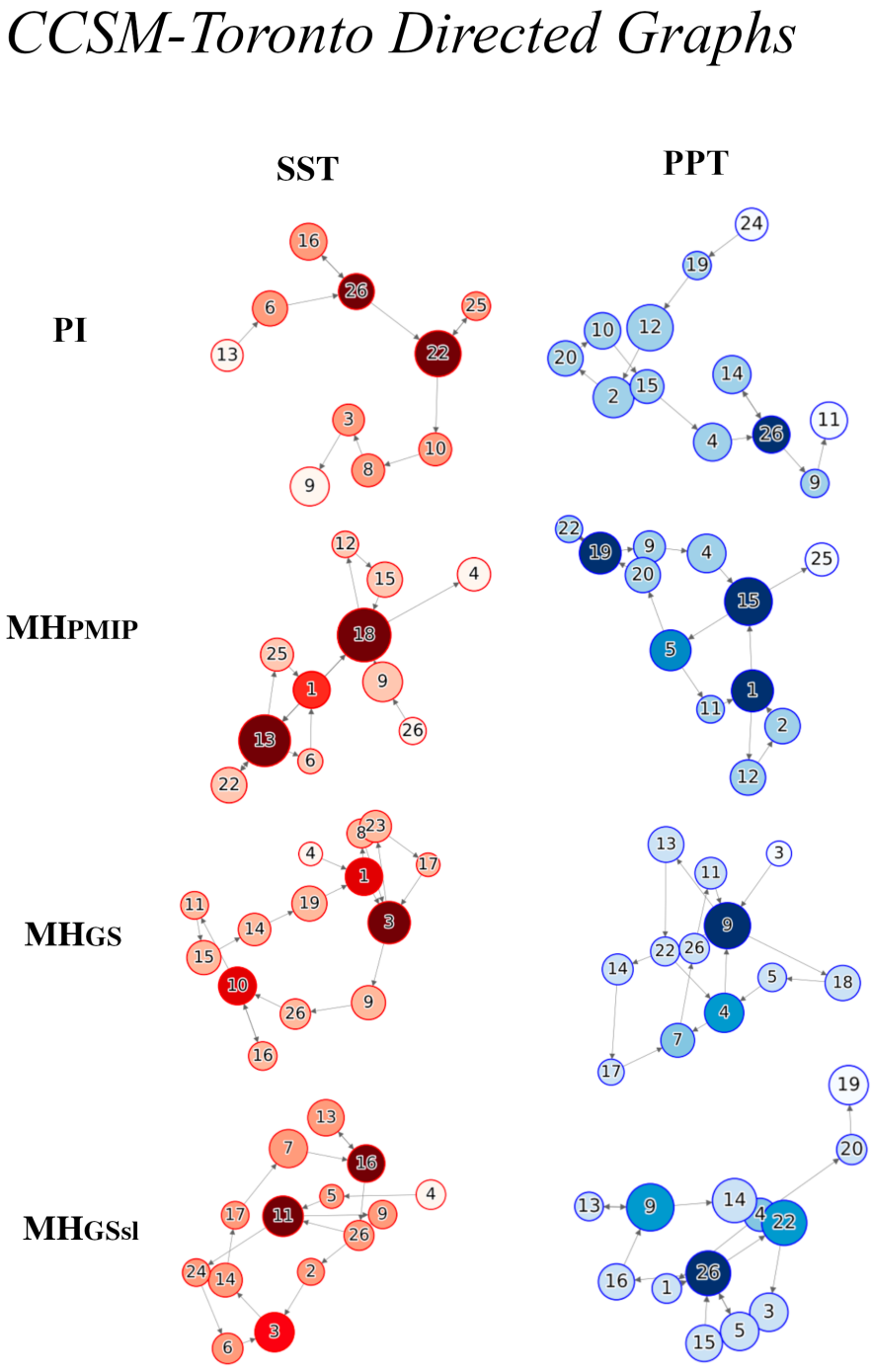

Figure 8. Directed graphs from CCSM-T - PI, MH_{PMIP}, MH_{GS}, and MH_{GSsl} with soil and lake input runs. The red graphs represent the evolution of the SST system~~evolution~~, ~~and~~ while the blue graphs represent the ~~precipitation~~ evolution of precipitation. Each node signifies a specific state, as depicted in Figure ~~S1~~ S2 from the Supplementary Material.

3.2 ~~Shannon's Entropy and Model Variability Analysis~~

Shannon's Entropy and Model Variability Analysis

In this study, Shannon's Entropy (H_{sst} and H_{ppt}) is used to assess the level of organization ~~within~~ of the tropical and South Atlantic ~~system based on its SST and precipitation PCs~~ given its possible states (as described in Equation 1).

Our choice to study ~~the decadal variability comes from the~~ decadal variability stems from the coupling between SST and precipitation ~~coupling~~ at this time scale (Gorenstein et al., 2023). Since these two variables are correlated and ~~have~~ exhibit a strong feedback interaction controlling the energy balance along the Equator (Schneider et al., 2014), we expect them to vary together, creating a distinguishable climate variability response to external forces. ~~From a broader perspective, the entropy calculation~~ The first two columns of Table 2 show the entropy calculated in the PC phase space ~~reflects the organization of the SST modes of variability and their precipitation counterparts in each simulation. From this point onward, we characterize climate variability in terms of the entropy of a simulation, reflecting the transition between different states. Table 2 shows the entropy~~ and its 95% confidence interval for each model experiment.

Despite differences in parameterizations and physics among models, each entropy was computed in a unified ~~PC phase~~ space (the states of every simulation were ~~computed using the same EOFs~~ calculated using the EOFs extracted from the merged dataset). All model experiments were simulated over the same duration (100 years), enabling comparisons across the different models.

As seen in Figure 9 and Table 2, the entropy values are approximately 3. This is due to the structure of our phase space: with three defined phases (positive, neutral, and negative) for each of the three principal components, the system has $3^3 = 27$ possible states. The maximum entropy (equation 1) of a discrete space such as this would result in $\ln(27) \approx 3.296$. Since the simulation's thresholds in phase space are individually tuned to yield its maximum possible entropy (see Methods), it naturally approaches ln(27).

EC-Earth

~~The~~ EC-Earth~~model exhibits the lowest SST variability~~ 's SST variability significantly drops from PI to the different MH scenarios (it reduces 5% in MH_{PMIP} and 7% in ~~the MH_{PI} run~~ (MH_{GS} in comparison to the PI), when dust reduction is applied its entropy recovers back to PI levels. The lowest SST entropy of all models and scenarios is measured during EC-Earth's MH_{GS} (blue triangles in Fig. 9 'a'), indicating that in this scenario the EC-Earth model simulates a more organized Atlantic SST system. The ~~SST and precipitation variability from this model show opposite responses to the Green Sahara vegetation when dust reduction is considered. In the Green Sahara experiment without dust reduction (MH_{GS}), the precipitation variability is low, and comparable to the PI run, while the SST variability is significantly higher (5% in comparison to the PI). In the experiment where both vegetation and dust reduction are considered (MH_{GSdr}), precipitation variability shows an increase (6% in comparison to the PI and 8% in comparison to MH_{GS}), while the SST variability decreases to PI standards~~precipitation variability shows no significant changes through all the different scenarios (blue triangles in Fig. 9 'b').

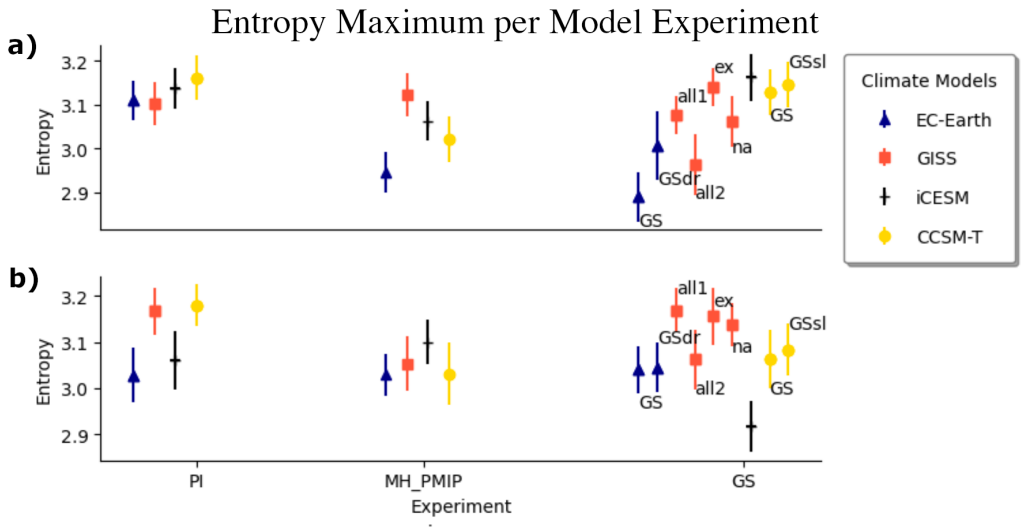

Figure 9. Maximum Entropy ~~mean~~ values and uncertainty for each model experiment ~~. Entropy values for~~ using the ~~SST~~ Atlantic Ocean PCs phase space, (a)~~and precipitation~~ : for SST; (b) for precipitation. From left to right: Pre-Industrial (PI); mid-Holocene only orbital forcing (MH_{PMIP}); and mid-Holocene with Green Sahara boundary conditions (MH_{GS}) experiments. All models include PI, MH_{PMIP}, and MH_{GS} runs. Under Green Sahara conditions, additional experiments include: EC-Earth (ECE) with northern African vegetation and dust reduction (dr); GISS with both extratropical and northern African vegetation (GISSall1 and GISSall2), with only extratropical vegetation (GISSex), and with only north African vegetation (GISSna); CCSM-T with soil and lakes (sl).

GISS

Compared to the PI experiment, GISS exhibits significant changes in ~~the SST variability only in the MH_{GSall1} and MH_{GSna} experiments~~ both SST and precipitation variability in the MH_{GSall2} experiment (5% in comparison to the PI). ~~While the precipitation variability has shown a decrease~~ Besides this simulation, only MH_{PMIP} shown significant precipitation variability decrease when compared to PI. In this model, the largest entropy difference comes from SST in MH_{GSall2} ~~(4% in comparison to the PI).~~ and MH_{GSex} (2.96 and 3.14, respectively - Table 2).

iCESM

For this model, the lowest decadal SST variability happens in the ~~PI experiment. The~~ MH_{PMIP} ~~and MH_{GS} show no~~ experiment (black hyfen in Figure 9), although without significant difference between ~~them, they both have 6% higher than PI decadal SST variability. However, the precipitation variability is higher in the MH_{PIMIP} experiment~~ the scenarios. The precipitation entropy shows significant decrese when vegetation is considered in the Sahara, MH_{GS} is the lowest of all simulations and scenarios (4% ~~higher~~ lower than the PI experiment and ~~9% higher than the MH_{GS}~~6% lower than the MH_{PMIP}).

The decadal SST variability is higher in the PI experiment, but ~~not~~ only significantly different from the ~~other experiments~~ MH_{PMIP} experiment (4% lower than the PI). Conversely, the MH_{PMIP}, MH_{GS} and MH_{GSsl} present 5% lower than PI precipitation variability.

3.2 The Green-Sahara Simulations in the Atlantic Ocean Modes' Phase Space

PC-based modes can sometimes blend physical processes or show sensitivity to the chosen spatial and temporal domains, requiring careful interpretation (Preisendorfer and Mobley, 1988). An alternative approach to reducing Atlantic SST dimensions into a 3D phase space uses regional SST indices. These averages provide simple, physically interpretable metrics of climate mode strength. To test how phase space definitions affect Shannon's Entropy, we repeat our calculations using indices for the Atlantic Meridional Mode, the Atlantic Equatorial Mode, and the South Atlantic Subtropical Dipole (AMM,AEM and SASD, see Methods); representing Atlantic decadal variability through a traditional oceanographic lens (Deser et al., 2010).

In the merged dataset, the first PC correlates strongly with the AEM (70%) and SASD (64%), while the second PC correlates with the AMM (71%). However, while the SST indices are significantly intercorrelated (39–43% in the merged dataset), the PCs maintain negligible correlation (below 3%). As an orthonormal basis, PCs inherently ensure minimal correlation between dimensions, unlike regional indices. This index-based phase space yields generally lower entropy values than the PC-based space. While Shannon Entropy does not directly measure correlation, if two PCs are correlated, their positive, neutral and negative phases vary togheter and the system ocuppies less states, resulting in lower entropy values.

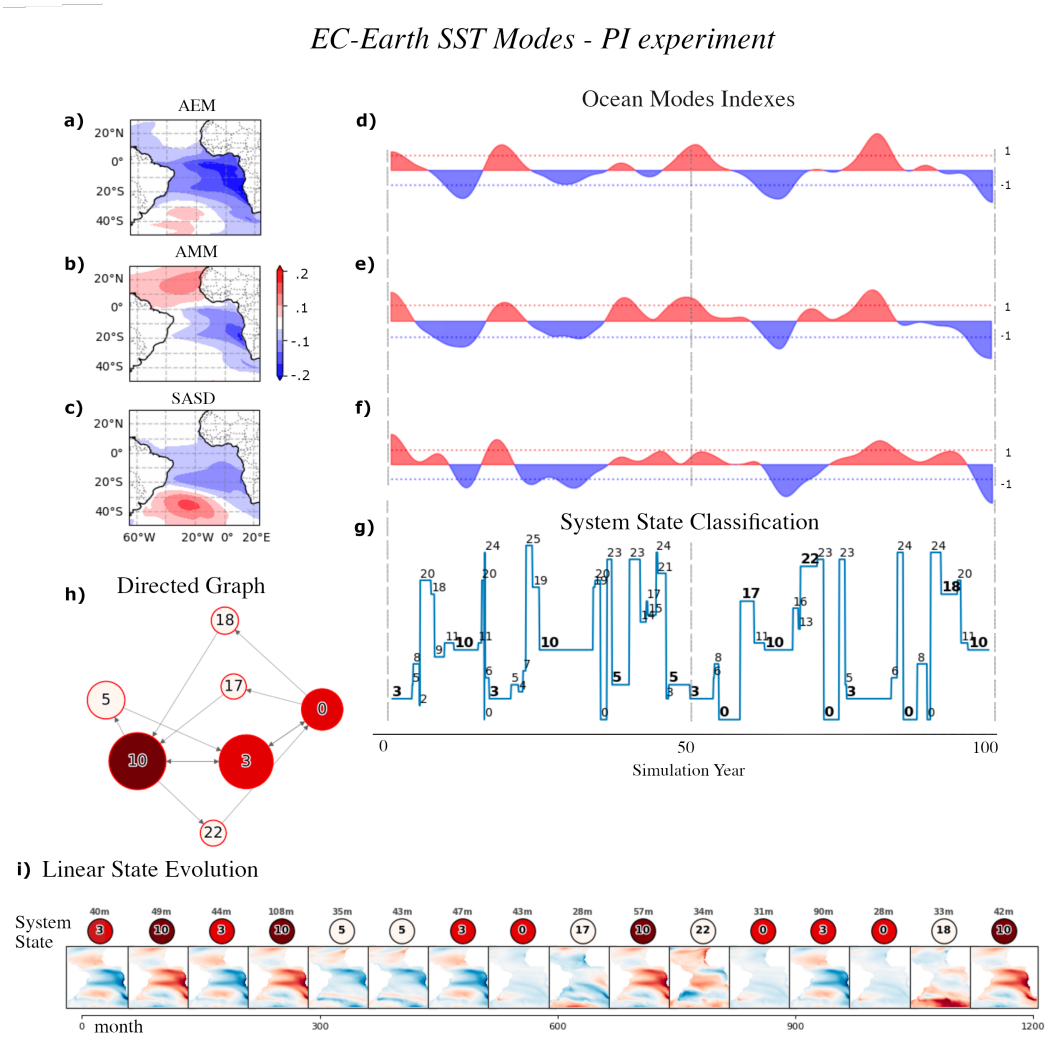

Figure 10. EC-Earth SST system state identification and evolution during the PI experiment. (a),(b), and (c): The merged ensemble AMM, AEM, and SASD, respectively; (d),(e), and (f): their respective index series, blue for negative and red for positive, dashed lines indicating the 1 standard deviation value. (g) The cluster identification of the discrete system state given the three above Ocean Mode indices, bold font used in the most persistent states (lasting more than 24 months); (h) illustrates state evolution of the most persistent states. (i) tracks the state evolution in linear form. Each node displays its cluster number, spatial pattern, and duration in months before transitioning.

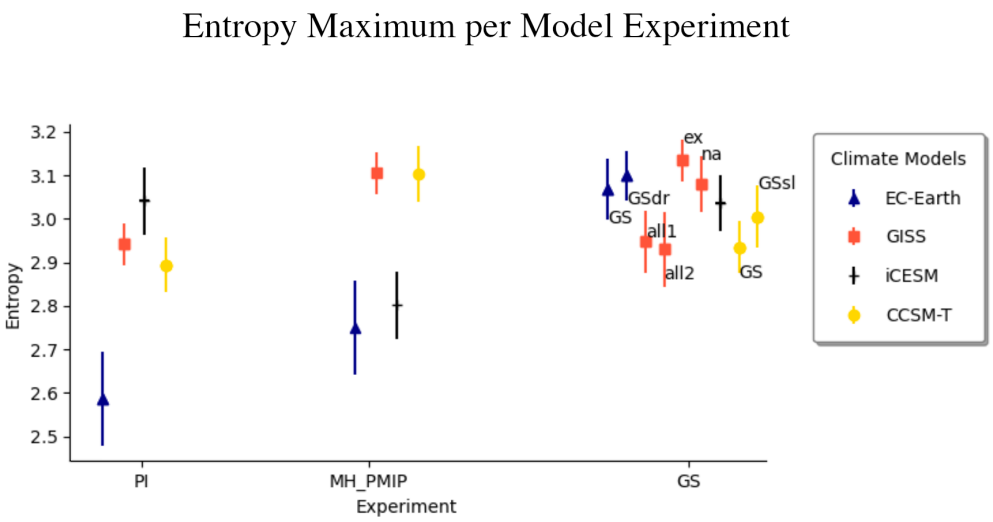

Figure 11. Maximum Entropy values and uncertainty for each model experiment for SST using the Atlantic Ocean modes phase space. From left to right: Pre-Industrial (PI); mid-Holocene only orbital forcing (MH_{PMIP}); and mid-Holocene with Green Sahara boundary conditions (MH_{GS}) experiments. All models include PI, MH_{PMIP}, and MH_{GS} runs. Under Green Sahara conditions, additional experiments include: EC-Earth (ECE) with northern African vegetation and dust reduction (dr); GISS with both extratropical and northern African vegetation (GISSall1 and GISSall2), with only extratropical vegetation (GISSex), and with only north African vegetation (GISSna); CCSM-T with soil and lakes (sl).

Table 2: Entropy mean and Standard Deviation using 1200 months long series from the model runs - calculated in the PC and Atlantic Ocean Modes phase spaces.

		Entropies in PC phase space		Entropies in Modes phase space
Model	Scenario	H_{sst}	H_{ppt}	H_{sst}
ECE	PI	3.11 ± 0.05	3.03 ± 0.06	2.59 ± 0.11
ECE	MH_{PMIP}	2.95 ± 0.06	3.03 ± 0.05	2.75 ± 0.08
ECE	MH_{GS}	2.89 ± 0.06	3.04 ± 0.05	3.07 ± 0.07
ECE	MH_{GSdr}	3.01 ± 0.08	3.05 ± 0.05	3.10 ± 0.06
GISS	PI	3.10 ± 0.05	3.17 ± 0.05	2.94 ± 0.05
GISS	MH_{PMIP}	3.12 ± 0.05	3.05 ± 0.06	3.11 ± 0.06
GISS	MH_{GSall1}	3.08 ± 0.04	3.17 ± 0.05	2.95 ± 0.07
GISS	MH_{GSall2}	2.96 ± 0.07	3.06 ± 0.06	2.93 ± 0.09
GISS	MH_{GSex}	3.14 ± 0.04	3.16 ± 0.06	3.13 ± 0.05
GISS	MH_{GSna}	3.06 ± 0.06	3.14 ± 0.05	3.08 ± 0.07
iCESM	PI	3.14 ± 0.05	3.06 ± 0.06	3.04 ± 0.08
iCESM	MH_{PMIP}	3.06 ± 0.06	3.10 ± 0.05	2.80 ± 0.09
iCESM	MH_{GS}	3.16 ± 0.05	2.92 ± 0.06	3.04 ± 0.06
CCSM-T	PI	3.16 ± 0.05	3.18 ± 0.05	2.89 ± 0.06
CCSM-T	MH_{PMIP}	3.02 ± 0.07	3.03 ± 0.07	3.10 ± 0.06
CCSM-T	MH_{GS}	3.13 ± 0.05	3.06 ± 0.06	2.93 ± 0.06
CCSM-T	MH_{GSsl}	3.15 ± 0.05	3.08 ± 0.06	3.01 ± 0.07

EC-Earth

The EC-Earth PI experiment (Figure 10) best illustrates how high correlation results in low entropy, showing the lowest entropy of all simulations within the Atlantic Ocean Modes phase space. In this specific setup, the AEM and AMM are correlated at 88%, while the AMM and SASD show a 76% correlation. Conversely, all MH scenarios exhibit higher entropy than the PI (6% for MH_{PMIP} and 19% for GS with/without dust) as these Atlantic modes decouple.

GISS

Compared with the PC phase space, GISS PI entropy reduces using the Atlantic ocean modes indices (Table 11). The entropy from the remaining MH scenarios mostly decreases; however, they show no significant changes to the entropies calculated in the PCs phase space.

iCESM

For this model, the SST entropies show a general decrease, while holding the same internal biases seen in the PC phase space entropies (Table 11).

CCSM-Toronto

The only significant difference is still between PI and MH_PMIP; however, in this phase space, MH_{PMIP} holds the largest entropy amongst this model's different experiments (7% higher than PI).

3.3 The Observational data Entropy

A primary goal of numerical climate models is the faithful reproduction of low-frequency decadal variability. Notable differences exist between the PCs extracted from observational data and model data, nor do they represent the same variance as the principal components from the leading components seen in the observational satellite era (Figure S1). However, the EOFs extracted from the merged simulations dataset can be projected onto the observational data time series. As long as they have the same length, the use of maximum Entropy enables a comparison between the observational data and the simulations' trajectories in a common phase space. Since the observational datasets range from 1980 to 2015, the results shown in the Table ahead are the Entropy values of the first 420 months (35 years) of each simulation. Within these time windows, the resulting entropy values are lower, indicating that shorter intervals do not fully capture the decadal variability envelope of the tropical and South Atlantic system.

Typically, satellite-era observations are compared against historical model runs. Previous research categorized the tropical and South Atlantic systems into a discrete evolution of patterns, tracking the SST and precipitation cycles using reanalysis data from $1890-2015$ with a directed graph format (Gorenstein et al., 2023). However, as an attempt to quantitatively compare the values emerging from the numerical climate models' entropy in these MH experiments, we calculate the entropy from two observational datasets (the HadISST and the GPCP datasets - see Methods). These values are presented in Table 3.

Table 3: Entropy mean and Standard Deviation from the 420-months-long series model runs and the observation data set

Model	Scenario	Entropies in PC phase space		Entropies in Modes phase space
		H_{sst}	H_{ppt}	H_{sst}
ECE	PI	2.60 ± 0.11	2.70 ± 0.08	2.26 ± 0.13
ECE	MH_{PMIP}	2.79 ± 0.09	2.91 ± 0.13	2.45 ± 0.10
ECE	MH_{GS}	2.63 ± 0.07	2.58 ± 0.09	2.80 ± 0.11
ECE	MH_{GSdr}	2.62 ± 0.09	2.80 ± 0.08	2.67 ± 0.09
GISS	PI	2.73 ± 0.08	2.95 ± 0.08	2.76 ± 0.09
GISS	MH_{PMIP}	2.75 ± 0.08	2.63 ± 0.10	2.81 ± 0.09
GISS	MH_{GSall1}	2.83 ± 0.10	2.78 ± 0.14	2.64 ± 0.10
GISS	MH_{GSall2}	2.85 ± 0.09	2.68 ± 0.10	2.62 ± 0.11
GISS	MH_{GSex}	2.95 ± 0.12	2.74 ± 0.10	3.04 ± 0.09
GISS	MH_{GSna}	2.80 ± 0.10	2.81 ± 0.11	2.72 ± 0.10
iCESM	PI	2.71 ± 0.10	2.72 ± 0.10	2.77 ± 0.09
iCESM	MH_{PMIP}	2.85 ± 0.09	2.79 ± 0.08	2.74 ± 0.12
iCESM	MH_{GS}	2.90 ± 0.11	2.71 ± 0.10	2.84 ± 0.09
CCSM-T	PI	2.90 ± 0.09	2.56 ± 0.17	2.72 ± 0.11
CCSM-T	MH_{PMIP}	2.57 ± 0.10	2.70 ± 0.07	2.57 ± 0.10
CCSM-T	MH_{GS}	2.57 ± 0.07	2.92 ± 0.13	2.73 ± 0.12
CCSM-T	MH_{GSsl}	2.65 ± 0.09	2.76 ± 0.10	2.83 ± 0.08
Observation	$1980 - 2015$	2.83 ± 0.09	2.78 ± 0.09	2.40 ± 0.13

In the PC phase space, the ensemble model mean (2.76 for SST and 2.75 for precipitation) falls within the observational entropy uncertainty interval. However, in the Atlantic Ocean Modes phase space, the ensemble model mean (2.70) is significantly higher than the observational entropy value (2.40 ± 0.13). While this could suggest that historical variability is lower than most of the PI and MH experiments presented, such a direct comparison assumes the models represent these modes accurately. Instead, this discrepancy may indicate that, for this methodology, studying Atlantic decadal variability in simulations is more reliable when using principal components rather than traditional SST indices.

4 Discussion

~~The standard approach to analyze~~ The core purpose of the developed methodology is to evaluate and compare the temporal variability of a physical system across different scenarios. For the tropical and South Atlantic specifically, pre-Industrial and mid-Holocene runs were chosen because they provide a period where multiple known forcings (such as insolation and vegetation) can be used to study the coupling and decadal dependencies between SST and precipitation.

The standard approach to analyzing these climate variables variability in climate reconstructions using ~~proxies and~~ numerical model simulations is to compute the two-dimensional mean and standard deviation fields, and frequency spectra ~~(Flato et al., 2014; Olonsch~~ (Flato et al., 2014; Olonscheck and Notz, 2017; Pendergrass et al., 2017; Bianchini et al., 2025). This approach accounts for the local dependencies of climate variables, where the standard deviation fields indicate the amplitude of regional variability, and the frequency spectra reveal periodicity.

~~Utilizing various types of~~ There is no trivial path to compare our results with the standard methodology, as the underlying concepts used to define climate variability differ, and although its not the main purpouse of our methodology, we can use it to validate the model climate simulations with proxy information. Previous studies have used biochemical proxy data from sediment and ice cores ~~, previous studies have examined~~ to examine mid-Holocene climate variability in the Tropical and South Atlantic ~~regions using the conventional methodology~~ (Debret et al., 2009; Wirtz et al., 2010). Wirtz et al. ~~,~~ (2010) found ~~that most of the tropical Atlantic exhibited~~ generally lower precipitation variability than at present, except ~~along~~ for the Northeast Brazil coast, where variability ~~was higher. Additionally, numerical climate models have been used to recreate ocean modes indexes and study~~ increased. Numerical models have also simulated ocean mode indices and monsoon changes in Africa ~~, America, and South America with~~ and the Americas using mid-Holocene ~~forcing parameters (Harrison et al., 2003; Zhao et al., 2007) . An analysis of nine coupled ocean-atmosphere general circulation model experiments from PMIP2 by~~ forcings (Harrison et al., 2003; Zhao . Specifically, Zhao et al. (2007) ~~indicated lower precipitation variability in the Sahel region during the mid-Holocene, with a weakening of~~ analyzed nine PMIP2 models, finding reduced Sahel precipitation variability and weakened teleconnections between Pacific/Atlantic ~~SST~~ SSTs and Tropical Atlantic precipitation, suggesting a decoupling of ~~precipitation and SST~~these variables.

~~Some of the model responses in our studyagree with a lower precipitation variability in the~~ In our study, most model responses show lower tropical and South Atlantic SST variability during the mid-Holocene ~~(specificallyfor CCSM-Toronto and iCESM's MH_{GS})and suggest~~ when using only insolation parameters; specifically, all MH_{PMIP} models exhibit lower Entropy than MH_{PI}, except for GISS, which shows equivalent values (Figure 9). However, only GISS and CCSM-T show lower precipitation variability in MH_{PMIP} compared to MH_{PI}. When Green Sahara vegetation is factored in, a decoupling between SST and precipitation variability ~~when mid-Holocene vegetation in the Green Sahara is factored in (as seen with~~ becomes clearer in three of the four models: EC-Earth~~). However, there is no trivial path for comparison between the standard methodology and ours, since the concepts used to define climate variability differ.~~ , iCESM, and CCSM-T show significantly larger entropy differences between the variables, though EC-Earth displays low SST entropy with high precipitation, while CCSM-T and iCESM show the reverse. In contrast, the GISS model keeps the variables more closely coupled, with no significant entropy differences across scenarios.

~~The standard approach is more closely related to data-science statistics, effectively identifying regions most vulnerable to variability changes, which facilitates model regional validation with~~ Measuring decadal variability in climate models typically relies on statistical methods common in data science to pinpoint regions highly susceptible to change, thereby aiding in the regional validation of models against observational data. However, recent research utilizing information theory suggests that traditional variance-based estimates can be unreliable when accounting for non-Gaussian higher statistical moments. Consequently, there is a growing need for variability metrics that remain robust regardless of a variable's amplitude or units of measurement (Sane et al., 2024). ~~In contrast, our~~ Our methodology measures a region's decadal climate variability concerning the chosen phase space (ocean modes of variability and their precipitation counterparts~~, aligning more closely with the classical concepts of~~). Although we have shown that it is more straight forward to use the leading PCs of SST in the tropical Atlantic Ocean for the absense of correlation between its orthonormal components, they still alow us to

study the Atlantic Ocean Modes as conceptualized in the classical oceanography, climatology, and dynamic systems theory (~~Deser et al., 2010; Ghil and Lucarini, 2020).~~ (Deser et al., 2010; Ghil and Lucarini, 2020; Cheung et al., 2026).

Modes such as El Niño, the AMM, and the AEM influence climate across the globe~~,~~ ; they are known to impact society (McGowan et al., 2012; Lam et al., 2019), agriculture (Anderson et al., 2018), the atmosphere (Xie and Carton, 2004; Gorenstein et al., 2023), and climate equilibrium (Pillai et al., 2022; Cai et al., 2021). ~~Their evolution is a more conceptual framework to measure, discuss, and compare numerical models ' decadal climate representation~~The temporal evolution of these modes provides a conceptual framework for measuring decadal climate variability in numerical models using the same metrics applied to observational datasets. Accordingly, the phase space used to compute Shannon entropy is constructed to explicitly reflect the variability associated with these climate modes. Although we employed standard deviation to define the positive, neutral, and negative phases of the Atlantic modes, it is not necessarily the case that a simulation with high regional standard deviation (the traditional measure of climate variability) will correspond to a high entropy measurement. ~~A simulation with high entropy exhibits oscillations between the states that define the discrete PC phase space.~~

5 Conclusions

~~Using the PC analysis to reduce the dimensionality of the data, we examine the decadal variability of Tropical~~ We introduce a information-theoretic framework to characterize the organization and variability of climate systems. We demonstrate our methodology by analyzing the tropical and South Atlantic SST and precipitation ~~across four different numerical models :~~ decadal variability across four climate models (EC-Earth, GISS, iCESM, and CESM-Toronto~~. We depict each simulation's~~) simulating the PI, mid-Holocene experiments and observational data from the satellite era (HadISST and GPCP). Representing SST and precipitation ~~trajectories within a reduced PC phase space. While directed graphs illustrating the trajectories are intriguing, they can be overly complex. Therefore, it is more effective to use them to calculate macro properties, such as Shannon's Entropy, which serve as measures of system organization and provide analogs for the decadal variability observed across these simulations~~as trajectories in a unified physically motivated low-dimensional phase space, we describe the tropical and South Atlantic climate system in a course-grained space of 27 possible states. In this discrete space, we compute Shannon's entropy, accesing how organized the coupled ocean–atmosphere system is under PI and different MH boundary conditions.

~~The highest entropy among the PI runs is observed in the CCSM-Toronto and GISS models, attributed to the system evolving into a greater number of states within a shorter time frame. Moreover, the difference between the four models in PI was not maintained across the different experiments, indicating a lack of consensus on the increase or decrease of variability in any specific experiment.~~ Across four models, the results show that mid-Holocene forcings can significantly alter the degree of organization of Atlantic decadal variability, with model-dependent entropy changes, and different SST and precipitation responses. Comparisons with observational datasets indicate that PC-based phase spaces provide a more consistent and robust basis for evaluating low-frequency Atlantic variability than traditional SST indices, highlighting entropy as a powerful metric to diagnose how external forcings reshape the structure, persistence, and transitions of dominant climate modes.

~~The CCSM-Toronto showed lower than PI precipitation variability in the MH_{PMIP} and MH_{GS} runs, but no significant changesin the SST variability amongst the different experiments. The~~ EC-Earth ~~climate variability exhibited high sensitivity to dust emissions and vegetation in the Green Sahara. Comparing MH_{PIMIP}~~ shows the strongest reduction in SST entropy under Green Sahara conditions, indicating a more organized and persistent Atlantic Ocean system that is partially reversed when dust reduction is included, while its precipitation variability remains largely unchanged. GISS displays a spread in entropy responses, with the MH_{GSall2} simulation exhibiting significant reductions in both SST and ~~MH_{GS}, the vegetated simulation increased the SST variability while reducing the precipitation variability. This behavior inverts when comparing the MH_{GS} and MH_{GSdr} runs: the dust reduction parametrization lowered the SST variability while increasing significantly the precipitation variability . The GISS model displayed the smallest precipitation entropy variation among all experiments, showing no significant differences. The SST variability shows significant differences between MH_{ex} and MH_{na}. Suggesting that the Atlantic SST variability increases with the presence of vegetation in North Africa, while the extra-tropical vegetation contributes to a decrease in SST variability. iCESM SST~~ precipitation entropy, highlighting the sensitivity of Atlantic variability ~~showed higher than PI variability in the MH_{PMIP} and MH_{GS} runs, and~~ to ocean–atmosphere coupling in this simulation. In contrast, iCESM exhibits comparatively muted SST entropy changes across scenarios but a clearer precipitation response under Green Sahara forcing, whereas CCSM-Toronto shows a tendency toward reduced precipitation variability across all mid-Holocene experiments, with weaker and more selective SST changes. Taken together, these results indicate that while the direction and magnitude of entropy changes depend on model physics and boundary-condition implementation, all models encode distinct and interpretable reorganizations of Atlantic decadal variability under altered Holocene climates.

Because this study is based on single realizations, differences in entropy between experiments may reflect a combination of sensitivity to initial conditions and differences in boundary conditions or parameterized processes. Applying this methodology to ensemble simulations or emulators that systematically perturb initial conditions and external forcings (e.g., dust or vegetation) represents a natural extension of this work and would enable a more rigorous assessment of how Shannon entropy responds to different climate variables and scenarios.

This methodology characterizes system dynamics and variability in terms of state occupancy and transitions rather than absolute anomaly magnitudes. By discretizing the climate system in a unified low-dimensional phase space and computing Shannon's Entropy, the ~~lowest entropy value of all models~~ underlying climate variability can be directly compared between different models, experiments, and observations. The approach captures how frequently the system revisits certain states, how persistent those states are, and ~~experiments in its precipitation entropy from the MH_{GS} experiment. When comparing the MH_{PMIP} and MH_{GS}, although the SST variability remained similar, the precipitation variability presented a significant decrease (9%, the largest entropy variation from simulations within the same model) . Indicating that the model's Tropical and South Atlantic precipitation variability has a high sensitivity to vegetation parametrization, however not directly affecting its SST variability.~~ how rich the transition structure is, all of which are fundamental aspects of variability that are not accessible through variance-based metrics alone. Moreover, because entropy is computed in a common phase space using the maximum entropy threshold, it provides a unified and scale-independent measure of organization that remains robust even when models differ in mean state, variance, or bias, thereby complementing traditional and well-established statistical diagnostics. This

makes the framework especially powerful for inter-model comparisons and for evaluating low-frequency climate variability across non-homogeneous datasets.

~~To define the decadal variability of a simulation, we used the probability distribution from the ocean modes and their precipitation counterparts. We employed this technique for model comparison, furthermore, our methodology can be used to study model biases and validation. Accurately simulating large patterns and climate oscillations around its mean state can be challenging for numerical models, the methodology presented in this study adds a valuable tool to the comprehensive analysis of climate models .~~

. Code Availability: The current version of the models used to produce the results used in this paper are available from: EC-Earth - (Döscher et al., 2021); iCESM - (Tabor et al., 2020); CCSM-Toronto - (Peltier and Vettoretti, 2014); GISS - (Schmidt et al., 2014). The exact simulation outputs used to produce the results used in this paper can be found in the following link https://github.com/IuriGorenstein/Entropy_MH_ESM, as are scripts to produce the plots for all the simulations presented in this paper (Gorenstein, 2025).

. All authors have made substantial contributions to this manuscript related to their areas of expertise.

. The authors declare that none of the authors has any competing interests.

. Acknowledgements

This study was financed in part by the Coordenação de Aperfeiçoamento de Pessoal de Nível Superior - Brasil (CAPES) - Finance Code 001; FAPESP 2019/08247-1.

The authors would like to thank Dr. Qiong Zhang for providing the EC-Earth mid-Holocene experiments, as well as the constructive comments and suggestions that improved this manuscript.

References

Adler, R., Huffman, G., Chang, A., Ferraro, R., Xie, P., Janowiak, J., Rudolf, B., Schneider, U., Curtis, S., Bolvin, D., Gruber, A., Susskind, J., and Arkin, P.: The Version 2 Global Precipitation Climatology Project (GPCP) Monthly Precipitation Analysis (1979-Present), 2003.

Anderson, W., Seager, R., Baethgen, W., and Cane, M.: Trans-Pacific ENSO teleconnections pose a correlated risk to agriculture, Agricultural and forest meteorology, 262, 298–309, 2018.

Atwood, A. R., Donohoe, A., Battisti, D. S., Liu, X., and Pausata, F. S.: Robust longitudinally variable responses of the ITCZ to a myriad of climate forcings, Geophysical Research Letters, 47, e2020GL088 833, 2020.

Berger: Milankovitch Theory and climate, AGU. Ressearch Letters, https://doi.org/10.1029/RG026i004p00624, 1988.

Berger, A.: Long-Term Variations of Daily Insolation and Quaternary Climatic Changes, Journal of the Atmospheric Sciences, 35, 2362–2367, https://doi.org/https://doi.org/10.1175/1520-0469(1978)035<2362:LTVODI>2.0.CO;2, 1978.

Bianchini, P. R., Prado, L. F., Yokoyama, E., Wainer, I., Gorenstein, I., and Pausata, F. S.: Precipitation patterns and variability in Tropical Americas during the Holocene, Palaeogeography, Palaeoclimatology, Palaeoecology, p. 112935, 2025.

Bonfils, C. and Santer, B.: Investigating the possibility of a human component in various pacific decadal oscillation indices, Clim Dyn, 37, 1457–1468, https://doi.org/10.1007/s00382-010-0920-1, 2011.

Bova, S., Rosenthal, Y., Liu, Z., Godad, S. P., and Yan, M.: Seasonal origin of the thermal maxima at the Holocene and the last interglacial, Nature, 589, 548–553, https://doi.org/https://doi.org/10.1038/s41586-020-03155-x, 2021.

Brady, E., Stevenson, S., Bailey, D., Liu, Z., Noone, D., Nusbaumer, J., Otto-Bliesner, B., Tabor, C., Tomas, R., Wong, T., et al.: The connected isotopic water cycle in the Community Earth System Model version 1, Journal of Advances in Modeling Earth Systems, 11, 2547–2566, 2019.

Bühler, J. C., Axelsson, J., Lechleitner, F. A., Fohlmeister, J., LeGrande, A. N., Midhun, M., Sjolte, J., Werner, M., Yoshimura, K., and Rehfeld, K.: Investigating stable oxygen and carbon isotopic variability in speleothem records over the last millennium using multiple isotope-enabled climate models, Climate of the Past, 18, 1625–1654, 2022.

Burkea, K. D., Williams, J. W., Chandler, M. A., Haywood, A. M., Lunt, D. J., and Otto-Bliesner, B. L.: Pliocene and Eocene provide best analogs for nearfuture climates, PNAS, https://doi.org/10.1073/pnas.1809600115, 2018.

Cai, W., Santoso, A., Collins, M., Dewitte, B., Karamperidou, C., Kug, J.-S., Lengaigne, M., McPhaden, M. J., Stuecker, M. F., Taschetto, A. S., et al.: Changing El Niño–Southern oscillation in a warming climate, Nature Reviews Earth & Environment, 2, 628–644, 2021.

Chandler, R. E., Barnes, C. R., and Brierley, C. M.: Characterizing Spatial Structure in Climate Model Ensembles, Journal of Climate, 37, 1053–1064, 2024.

Cheung, A. H., Sane, A., and Fox-Kemper, B.: Understanding the characteristics and drivers of Pacific decadal variability in the Community Earth System Model Last Millennium Ensemble, Climate Dynamics, 64, 35, 2026.

Colose, C. M., LeGrande, A. N., and Vuille, M.: The influence of volcanic eruptions on the climate of tropical South America during the last millennium in an isotope-enabled general circulation model, Climate of the Past, 12, 961–979, 2016.

Debret, M., Sebag, D., Crosta, X., Massei, N., Petit, J.-R., Chapron, E., and Bout-Roumazeilles, V.: Evidence from wavelet analysis for a mid-Holocene transition in global climate forcing, Quaternary Science Reviews, 28, 2675–2688, 2009.

Demenocal, P., Ortiz, J., Guilderson, T., Adkins, J., Sarnthein, M., Baker, L., and Yarusinsky, M.: Abrupt onset and termination of the African Humid Period:: rapid climate responses to gradual insolation forcing, Quaternary science reviews, 19, 347–361, 2000.

Deser, C., Alexander, M. A., Xie, S.-P., and Phillips, A. S.: Sea Surface Temperature Variability: Patterns and Mechanisms, Annual Review of Marine Science, 2, 115–143, https://doi.org/10.1146/annurev-marine-120408-151453, pMID: 21141660, 2010.

Deser, C., Phillips, A., Bourdette, V., and Teng, H.: Uncertainty in climate change projections: the role of internal variability, Climate dynamics, 38, 527–546, 2012.

Dhrubajyoti, S., Karnauskas, K. B., and Goodkin, N. F.: Tropical Pacific SST and ITCZ Biases in Climate Models: Double Trouble for Future Rainfall Projections?, AGU, Geophys. Res. Lett., https://doi.org/10.1029/2018GL081363, 2019.

Diciccio, T. J. and Romano, J. P.: A review of bootstrap confidence intervals, Journal of the Royal Statistical Society: Series B (Methodological), 50, 338–354, 1988.

Döscher, R., Acosta, M., Alessandri, A., Anthoni, P., Arneth, A., Arsouze, T., Bergmann, T., Bernadello, R., Bousetta, S., Caron, L.-P., et al.: The EC-earth3 Earth system model for the climate model intercomparison project 6, Geoscientific Model Development Discussions, 1, 2021, 2021.

Flato, G., Marotzke, J., Abiodun, B., Braconnot, P., Chou, S. C., Collins, W., Cox, P., Driouech, F., Emori, S., Eyring, V., et al.: Evaluation of climate models, pp. 741–866, Cambridge University Press, 2014.

Froyland, G., Giannakis, D., Lintner, B. R., Pike, M., and Slawinska, J.: Spectral analysis of climate dynamics with operator-theoretic approaches, Nature communications, 12, 6570, 2021.

Ghil, M. and Lucarini, V.: The physics of climate variability and climate change, Reviews of Modern Physics, 92, 035 002, 2020.

Ghil, M., Allen, M. R., Dettinger, M. D., Ide, K., Kondrashov, D., Mann, M. E., Robertson, A. W., Saunders, A., Tian, Y., Varadi, F., et al.: Advanced spectral methods for climatic time series, Reviews of geophysics, 40, 3–1, 2002.

Gorenstein, I.: Code and Data for Calculating Entropy in Mid-Holocene Simulations of Earth System Models, https://github.com/IuriGorenstein/Entropy_MH_ESM, 2025.

Gorenstein, I., Prado, L. F., Bianchini, P. R., Wainer, I., Griffiths, M. L., Pausata, F. S., and Yokoyama, E.: A fully calibrated and updated mid-Holocene climate reconstruction for Eastern South America, Quaternary Science Reviews, 292, 107 646, 2022a.

Gorenstein, I., Wainer, I., Mata, M. M., and Tonelli, M.: Revisiting Antarctic sea-ice decadal variability since 1980, Polar Science, 31, 100 743, 2022b.

Gorenstein, I., Wainer, I., Pausata, F. S., Prado, L. F., Khodri, M., and Dias, P. L. S.: A 50-year cycle of sea surface temperature regulates decadal precipitation in the tropical and South Atlantic region, Communications Earth & Environment, 4, 427, 2023.

Harrison, S. P. a., Kutzbach, J. E., Liu, Z., Bartlein, P. J., Otto-Bliesner, B., Muhs, D., Prentice, I. C., and Thompson, R. S.: Mid-Holocene climates of the Americas: a dynamical response to changed seasonality, Climate Dynamics, 20, 663–688, 2003.

Haykin, S.: Neural Networks and Machine Learning, 2009.

Hinkley, D. V.: Bootstrap methods, Journal of the Royal Statistical Society: Series B (Methodological), 50, 321–337, 1988.

Hounsou-Gbo, G. A., Servain, J., Araujo, M., Caniaux, G., Bourlès, B., Fontenele, D., and Martins, E. S. P.: SST indexes in the Tropical South Atlantic for forecasting rainy seasons in Northeast Brazil, Atmosphere, 10, 335, https://doi.org/10.3390/atmos10060335, 2019.

Huo, Y., Peltier, W. R., and Chandan, D.: Mid-Holocene monsoons in South and Southeast Asia: dynamically downscaled simulations and the influence of the Green Sahara, Clim. Past, 17, 1645–1664, https://doi.org/https://doi.org/10.5194/cp-17-1645-2021, 2021.

Hurrell, J. W., Holland, M. M., Gent, P. R., Ghan, S., Kay, J. E., Kushner, P. J., Lamarque, J.-F., Large, W. G., Lawrence, D., Lindsay, K., et al.: The community earth system model: a framework for collaborative research, Bulletin of the American Meteorological Society, 94, 1339–1360, 2013.

Jolliffe, I.: Principal component analysis. New York: Springer-Verlag, 2002.

Kaufman, D., McKay, N., Routson, C., Erb, M., Davis, B., Heiri, O., Jaccard, S., Tierney, J., and Zhilich, . . S.: A global database of Holocene paleotemperature records, Scientific Data, https://doi.org/10.6084/m9.figshare.11967924, 2020.

Kiang, N. Y.-l.: Savannas and seasonal drought: the landscape-leaf connection through optimal stomatal control, University of California, Berkeley, 2002.

Kwiecien, O., Braun, T., Brunello, C. F., Faulkner, P., Hausmann, N., Helle, G., Hoggarth, J. A., Ionita, M., Jazwa, C. S., Kelmelis, S., Marwan, N., Nava-Fernandez, C., Nehme, C., Opel, T., Oster, J. L., Perşoiu, A., Petrie, C., Prufer, K., Saarni, S. M., Wolf, A., and Breitenbach, S. F.: What we talk about when we talk about seasonality – A transdisciplinary review, Earth-Science Reviews, 225, 103 843, https://doi.org/https://doi.org/10.1016/j.earscirev.2021.103843, 2022.

Lam, H. C. Y., Haines, A., McGregor, G., Chan, E. Y. Y., and Hajat, S.: Time-series study of associations between rates of people affected by disasters and the El Niño Southern Oscillation (ENSO) cycle, International journal of environmental research and public health, 16, 3146, 2019.

LeGrande, A. N. et al.: Stability of ENSO and its tropical Pacific teleconnections over the Last Millennium, 2015.

Lehner, F., Deser, C., Maher, N., Marotzke, J., Fischer, E. M., Brunner, L., Knutti, R., and Hawkins, E.: Partitioning climate projection uncertainty with multiple large ensembles and CMIP5/6, Earth System Dynamics, 11, 491–508, 2020.

Liu, Z., Harrison, S. P., Kutzbach, J., and Otto-Bliesner, B.: Global monsoons in the mid-Holocene and oceanic feedback, Climate Dynamics, 22, 157–182, https://doi.org/10.1007/s00382-003-0372-y, 2002.

Liu, Z., Harrison, S. P., Kutzbach, J., and Otto-Bliesner, B.: Global monsoons in the mid-Holocene and oceanic feedback, Climate Dynamics, 22, 157–182, https://doi.org/https://doi.org/10.1007/s00382-003-0372-y, 2004.

Mantua, N., Hare, S., Zhang, Y., Wallace, J., and Francis, R.: A Pacific interdecadal oscillation with impacts on salmon production, Bull Am Met Soc, 58, 1069–1079, 1997.

McGowan, H., Marx, S., Moss, P., and Hammond, A.: Evidence of ENSO mega-drought triggered collapse of prehistory Aboriginal society in northwest Australia, Geophysical Research Letters, 39, 2012.

Olonscheck, D. and Notz, D.: Consistently estimating internal climate variability from climate model simulations, Journal of Climate, 30, 9555–9573, 2017.

Pausata, F. S. R., Messori, G., and Zhang, Q.: Impacts of dust reduction on the northward expansion of the African monsoon during the Green Sahara period, Earth and Planetary Science Letters, 434, 298–307, https://doi.org/10.1016/j.epsl.2015.11.049, 2016.

Peltier, W. R. and Vettoretti, G.: Dansgaard-Oeschger oscillations predicted in a comprehensive model of glacial climate: A "kicked" salt oscillator in the Atlantic, Geophysical Research Letters, 41, 7306–7313, 2014.

Pendergrass, A. G., Knutti, R., Lehner, F., Deser, C., and Sanderson, B. M.: Precipitation variability increases in a warmer climate, Scientific reports, 7, 17 966, 2017.

Pillai, P. A., Dhakate, A. R., Ramu, D., et al.: The predictive role of spring season Atlantic Meridional Mode (AMM) in Indian Summer Monsoon Rainfall (ISMR) variability during the recent decades, 2022.

Preisendorfer, R. W. and Mobley, C. D.: Principal component analysis in meteorology and oceanography, Developments in atmospheric science, 17, 1988.

Rayner, N., Parker, D., and Horton, E.: Hadley Centre for Climate Prediction and Research, Met Office, Bracknell, UK global analyses of sea surface temperature, https://doi.org/10.1029/2002JD002670, 2003a.

Rayner, N. A., Parker, D. E., Horton, E., Folland, C. K., Alexander, L. V., Rowell, D., Kent, E. C., and Kaplan, A.: Global analyses of sea surface temperature, sea ice, and night marine air temperature since the late nineteenth century, Journal of Geophysical Research: Atmospheres, 108, 2003b.

Sane, A., Fox-Kemper, B., and Ullman, D. S.: Internal versus forced variability metrics for general circulation models using information theory, Journal of Geophysical Research: Oceans, 129, e2023JC020 101, 2024.

Sang, Y.-F.: Wavelet entropy-based investigation into the daily precipitation variability in the Yangtze River Delta, China, with rapid urbanizations, Theoretical and Applied Climatology, 111, 361–370, 2013.

Schmidt, G. A., Kelley, M., Nazarenko, L., Ruedy, R., Russell, G. L., Aleinov, I., Bauer, M., Bauer, S. E., Bhat, M. K., Bleck, R., et al.: Configuration and assessment of the GISS ModelE2 contributions to the CMIP5 archive, Journal of Advances in Modeling Earth Systems, 6, 141–184, 2014.

Schneider, T., Bischoff, T., and Haug, G. H.: Migrations and dynamics of the intertropical convergence zone, Nature, 513, 45–53, 2014.

Smith and Mayle, F. E.: Impact of mid- to late Holocene precipitation changes on vegetation across lowland tropical South America: a paleo-data synthesis, Quaternary Research, p. 1–22, https://doi.org/10.1017/qua.2017.89, 2017.

Smith, B., Wårlind, D., Arneth, A., Hickler, T., Leadley, P., Siltberg, J., and Zaehle, S.: Implications of incorporating N cycling and N limitations on primary production in an individual-based dynamic vegetation model, Biogeosciences, 11, 2027–2054, 2014.

Sohoulande, C.: Predictive Model for Characterizing Bioclimatic Variability within Köppen-Geiger Global Climate Classification Scheme, in: ASA, CSSA, SSSA International Annual Meeting, ASA-CSSA-SSSA, 2023.

Sun, Q., Miao, C., Duan, Q., Ashouri, H., Sorooshian, S., and Hsu, K.: A Review of Global Precipitation Data Sets: Data Sources, Estimation, and Intercomparisons, AGU - Reviews of Geophysics, https://doi.org/https://doi.org/10.1002/2017RG000574, 2017.

Tabor, C., Otto-Bliesner, B., and Liu, Z.: Speleothems of South American and Asian monsoons influenced by a Green Sahara, Geophysical Research Letters, 47, https://doi.org/10.1029/2020GL089695, 2020.

Wanner, H., Beer, J., Bütikofer, J., Crowley, T. J., Cubasch, U., Flückiger, J., Goosse, H., Grosjean, M., Joos, F., Kaplan, J. O., Küttel, M., Müller, S. A., Prentice, I. C., Solomina, O., Stocker, T. F., Tarasov, P., Wagner, M., and Widmann, M.: Mid- to Late Holocene climate change: an overview, Quaternary Science Reviews, 27, 1791–1828, https://doi.org/https://doi.org/10.1016/j.quascirev.2008.06.013, 2008.

Wirtz, K. W., Lohmann, G., Bernhardt, K., and Lemmen, C.: Mid-Holocene regional reorganization of climate variability: Analyses of proxy data in the frequency domain, Palaeogeography, Palaeoclimatology, Palaeoecology, 298, 189–200, 2010.

Wyser, K., van Noije, T., Yang, S., von Hardenberg, J., O'Donnell, D., and Döscher, R.: On the increased climate sensitivity in the EC-Earth model from CMIP5 to CMIP6, Geoscientific Model Development, 13, 3465–3474, 2020.

Xie, S.-P. and Carton, J. A.: Tropical Atlantic variability: Patterns, mechanisms, and impacts, Earth's Climate: The Ocean–Atmosphere Interaction, Geophys. Monogr, 147, 121–142, 2004.

Zhang, Y., Wallace, J., and Battisti, D.: ENSO-like interdecadal variability: 1900–93's, J Clim, 10, 1004–1020, 1997.

Zhao, Y. and Harrison, S.: Mid-Holocene monsoons: a multi-model analysis of the interhemispheric differences in the responses to orbital forcing and ocean feedbacks, Clim Dy, 39, 1457–1487, https://doi.org/10.1007/s00382-011-1193-z, 2012.

Zhao, Y., Braconnot, P., Harrison, S., Yiou, P., and Marti, O.: Simulated changes in the relationship between tropical ocean temperatures and the western African monsoon during the mid-Holocene, Climate Dynamics, 28, 533–551, 2007.